EXPERIMENTAL INVESTIGATION OF ELECTRON-PHONON INTERACTIONS IN SEMICONDUCTORS

FINAL REPORT

(December 16, 1966 - January 30, 1968)

by

Dr. Joseph P. Martin, Principal Investigator

Research Institute for Advanced Studies
(RIAS)
Martin Marietta Corporation
1450 South Rolling Road
Baltimore, Maryland 21227

January 1968

Contract No. NAS8-21046 ff 653 July 65

Control No. DCN 1-7-28-00018-01 (1F)

EXPERIMENTAL INVESTIGATION OF ELECTRON-PHONON INTERACTIONS IN SEMICONDUCTORS

FINAL REPORT

(December 16, 1966 - January 30, 1968)

by

Dr. Joseph P. Martin, Principal Investigator

Research Institute for Advanced Studies
(RIAS)
Martin Marietta Corporation
1450 South Rolling Road
Baltimore, Maryland 21227

January 1968

Contract No. NAS8-21046
Control No. DCN 1-7-28-00018-01 (1F)

Acknowledgments

This report was prepared by the RIAS Division, Martin Marietta Corporation under contract NAS8-21046, "Experimental Investigation of Electron-Phonon Interactions in Semiconductors" for the George C. Marshall Space Flight Center of the National Aeronautics and Space Administration. The work was administered under the technical direction of the Research Projects Laboratory, George C. Marshall Space Flight Center with Mr. William J. Robinson acting as project manager.

The author acknowledges with sincere thanks the extensive help from Dr. James B. Mead in both the experimental work and the theoretical discussion and interpretation of these studies. The technical assistance of Guy H. Parr throughout the program was absolutely essential. The electron-diffraction results were obtained with the help of John D. Venables and Michael Meyerhoff. Dr. Louis Witten provided continuing interest and insights. Dr. Donald Denburg provided helpful discussions and ideas on experimental techniques.

Table of Contents

I.	Introduction	2
II.	Sample Preparation	5
III.	CdS Transducer Preparation	9
	1. Quartz crystal microbalance and substrate holder	10
	2. Ion bombardment cleaning	15
	3. Evaporation procedure	17
	4. Evaluation of CdS film	18
	a. examination of interference fringes	18
	b. electron beam diffraction studies of film orientation	21
	c. acoustic tests of CdS transducers	25
IV.	Theory of Electron-Phonon Interactions	28
V.	Phonon Propagation in InSb	35
	1. InSb - C1	35
	2. InSb - D3b, -D3e, - C2b	41
	3. InSb - E7i 0.825 cm long	45
VI.	Hot Electron Effects	46
VII.	Summary and Conclusions	52

Abstract

Techniques for aligning, polishing and cutting semiconductor crystal rods for use in acoustic propagation studies of electron-phonon interaction were evolved. A CdS vapor-deposition system was set up for production of thin film transducers. The development of the system included a quartz crystal microbalance for measurement of film growth rate as well as an indirect ion-bombardment cleaning system. Reflection electron diffraction was used to determine that highly polished substrate surfaces were found to be necessary for oriented film growth. The transduction efficiency of the films grown to date is about 10 lb less than that obtained with x-cut quartz transducers. Electron heating effects on mobility were measured to evaluate their effect on theoretical predictions of acoustic gain. The electron heating data was used to obtain measures of energy relaxation time of the electrons. This relaxation time was found to be strongly dependent on electron temperature (4×10^{-7} sec at 4.2°K to 8×10^{-10} sec at 28°) and independent of lattice temperature. Analysis of measurements of temperature dependence of acoustic attenuation yielded values of absolute attenuation of 12 db/cm at 4.2°K and of acoustoelectric coupling coefficient of $K^2 = 3.3 \times 10^{-4}$. Preliminary measurements of attenuation as a function of applied electric field in InSb indicated a definite decrease in attenuation with increasing field.

I. INTRODUCTION

Measurement of the characteristics of propagation of mechanical waves through solids has served as an extremely useful technique in investigating the physical properties of matter in the solid state. In particular, the interaction of acoustic waves (or phonons when quantum mechanical effects become important) with conduction electrons has been a very instructive device. A great deal of theoretical work[1-6] has been done on the attenuation and amplification of ultrasonic waves and the related acousto-electric effect via the electron-phonon interaction, but relatively little experimental verification of this work has been achieved. A considerable amount of work at lower ultrasonic frequencies has been done with CdS, the material in which ultrasonic amplification was first demonstrated[7]. Some work on GaAs[8] demonstrated a moderate gain from 30 MHz to 90 MHz via the piezoelectric interaction. Amplification[9] of 9 GHz phonons in germanium was achieved through the deformation potential interaction where the multivalley nature of Ge prevented the space charge bunching which otherwise reduces the gain obtainable via deformation potential coupling.

It is the purpose of the present program to come to a better understanding of the interactions between electrons and phonons in semiconductors since this interaction is at the heart of the whole theory of the transport properties of solids. This interaction is studied experimentally by measuring the attenuation and gain of a coherent acoustic wave propagating through semiconductor crystals. The work

here has concentrated on InSb and represents further development of the studies reported in a previous technical report[10]. The method used in these experiments for studying this interaction involves conversion of microwave energy into a coherent phonon wave and then reconverting these phonons back into a microwave signal for detection and measurement. The interaction between phonons and conduction electrons can be affected by the electron drift velocity such that the phonon wave can be amplified or attenuated by the electrons in an amount depending on their velocity. This characteristic suggests that techniques related to those used in these experiments could find applications in microwave technology such as amplifiers, delay lines and modulators.

In the previous work[10] the piezoelectric method of generating acoustic waves was chosen over the magnetostrictive method. Some measurements were made to determine the characteristics of quartz and tourmaline crystals as transducers at 9.3 GHz. The transduction efficiency and the temperature dependence of phonon attenuation were measured for a number of such crystals. A large variability was observed from one crystal to another in transduction efficiency. However, the temperature dependence of phonon attenuation was very consistent from one crystal to another although the quartz and tourmaline results differed markedly from each other. The quartz data were in good agreement with the results of other investigators whose data covered portions of the dynamic range of this experiment[11,12]. None of the existing theories of phonon-phonon scattering appeared completely adequate to describe the data, but that of Maris[13] appeared to give the basic behavior which we observed

in both quartz and tourmaline, viz: an increase in slope of the temperature dependence of attenuation with decrease in temperature.

Quartz crystals were used as transducers to generate microwave phonons in high purity, n-type InSb semiconductor crystals in the previous work. Repeated attempts at detecting phonons failed with crystals cut from two boat-grown InSb ingots. These crystals both had a very high dislocation density, characteristic of boat grown crystals. A crystal cut from a third ingot which had been Czochralski grown with very low dislocation density was successful in propagating the 9.3 GHz phonons which were easily detectable in our system. A decrease in attenuation with increase in temperature between $4.2^{\circ}K$ and $15^{\circ}K$ was observed with this crystal. Such a decrease which is expected from phonon scattering by electrons was very large (up to 14 db change) and was reproducible qualitatively but not quantitatively. This is due to the complicated interference effects observed in the echo patterns and also due to the non-reproducibility of these interference patterns from one thermal cycle to another.

Another effect which was observed with this crystal was a frequency shift in the phonons which had traversed the InSb. This was detected by noting that in the super-heterodyne receiver system, a slightly higher (about 1-2 MHz) local oscillator frequency was required to maximize the signals corresponding to acoustic paths through the InSb as compared to those through the quartz transducer alone. The effect was quite pronounced and easily detectable.

The InSb crystal which gave the results discussed above was too short to effectively attach current leads for testing of the gain inter-

action. Therefore the principal thrust of the present work was to obtain acoustic propagation in InSb crystals which were long enough to attach current leads.

II. SAMPLE PREPARATION

The methods used for preparation of InSb crystals for acoustic propagation measurements are similar in some respects to those reported in the previous work[10], but a number of improvements in the technique were incorporated in the method. Two ingots were used in the process of this work and will be referred to as ingots D* and E/. The ingots were both n-type Czochalski grown with low dislocation density and with carrier concentration quoted at $N \sim 10^{14}$ cm^{-3}.

The method finally evolved for sample preparation and used with ingot E began with x-ray alignment of the ingot on a Laue diffraction camera to determine the direction of a (111) axis to $\pm 2^{\circ}$. The ingot was then lapped to produce two opposite faces normal to this axis. One face was then checked with a precision x-ray spectrogoniometer described previously[10] and lapping was repeated and alternated with spectrogoniometer checks until the surface was normal to the (111) axis to within 4 minutes of arc. Then this surface was polished with a high grade optical finish7/, flat to ~ 500 Å over the 2.5 cm diameter of the ingot. The opposite face was then lapped and polished to the same flatness and finish and also parallel to the first face to within 6 seconds of arc.

---

* Obtained from Cominco Products, Inc., Spokane, Washington 99201
/ Obtained from Nuclear Elements Corp., Butler, Pennsylvania 16001
7/ Polishing done by Muffoletto Optical Company, Baltimore, Maryland 21206

The ingot was then carefully cleaned in preparation for evaporation of cadmium sulfide transducer films. This consisted of washing in concentrated HCl, followed by distilled water, acetone, methanol and finally Freon* precision cleaning agent. The final step in the cleaning process consisted of ion bombardment in the vacuum chamber prior to CdS evaporation. Thin films of cadmium sulfide were then deposited on both faces and measured for thickness. The ion bombardment cleaning and CdS film deposition will be described more fully in Section IV.

Finally the ingot was mounted between two glass plates with red sealing wax completely covering both faces for cutting of rods. Then rods of 0.125" and 0.250" diameter were cut from the ingot parallel to the surface normal with an ultrasonic impact grinder†. The rods were then ready for insertion in the microwave cavity for acoustic testing.

Some of the InSb rods were glued to quartz crystals to use this method of piezoelectric excitation rather than the CdS film. The method used for gluing the crystals started with the same careful cleaning procedure described above for the CdS film evaporation except that no ion-bombardment cleaning was used. The quartz and InSb rods were then placed together and the interface examined in monochromatic light for interference fringes. After several recleanings it was possible to get the surfaces free of dirt such that the two surfaces would have less than one interference fringe. The two rods were care-

---

* E.I. Dupont de Nemours Inc.-Freon Products Div., East Orange, N.J. 07017

† Raytheon Model 2-334-20, CA&S Division, Waltham, Massachusetts

fully placed between the jaws of an indicating micrometer* with dial readings of 10^{-4} inches (2.54 microns). It was possible to estimate readings to .25 microns. After recording the dial reading the rods were removed, a spot of epoxy resin≠ placed on the interface, and replaced in the micrometer. The micrometer was then tapped lightly until the reading returned to its previous value indicating that the film was less than .25 microns thick and probably reasonably parallel.

It was necessary to attach leads to the crystals for applying the electric fields used in obtaining the necessary electron drift velocities. The electrical contacts could not be made on the end faces of the rods since these had to be preserved for acoustic transmission and reflection. The leads were therefore attached around the ends of the rod. After first attaching the leads with solder using an ultrasonic soldering tool, it was found that they could be attached more accurately with silver paint**. The conductivity measurements described in Section VI showed the same results as with soldered contacts. The electrical contacts were constructed from 0.015" diameter phosphor bronze wire coiled into a circular loop over a form with a diameter smaller than the crystal rod. Then this coiled loop was opened enough to be sprung onto the InSb rod as seen in Fig. 1. Voltage probe contacts made of 0.005" diameter copper wire and attached with silver paint were spaced 0.13 cm apart near the center of the rod to measure the resistivity of the sample. To prevent these contacts from breaking loose, they were

---

* Etalon Dial Micrometer #25, Alina Corp., Plainview, L.I., New York 11803

≠ Eccobond 45 LV with Catalyst 15 LV - Emerson & Cummings, Inc. Gardena, California

** Conductive Silver #481, E.I. duPont de Nemours & Co., Electrochemicals Dept., Wilmington, Delaware

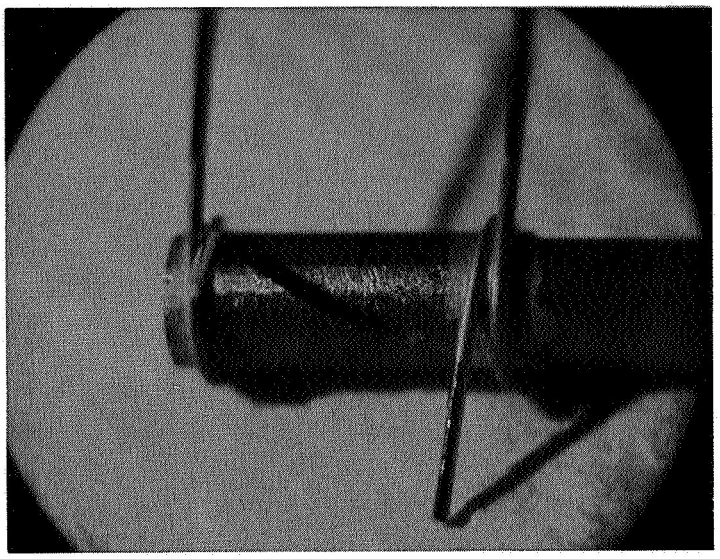

Figure 1 - Photograph showing the InSb rod E-7i glued to quartz transducer QV6 with electrical contacts attached with silver conducting paint.

covered with a foaming epoxy[Δ] which holds them firmly but without exerting undue thermal strain.

III. CdS TRANSDUCER PREPARATION

In previous work at this laboratory, x-cut quartz rods glued to the semiconductors served as transducers[10]. This method led to rather severe acoustic interference effects arising from slight deviations from parallelism and flatness of the bonded faces. Although the parallelism and flatness of a crystal can be maintained within tolerable limits (about 10% of the acoustic wavelength of ~ 5000 Å) during polishing, it is very difficult to maintain these limits between two bonded faces of dissimilar materials when the temperature is varied over a wide range. To circumvent this problem, a system was constructed and techniques were adapted for producing thin film transducers to replace the quartz crystals. The method developed[14] by deKlerk for producing thin film piezoelectric transducers of very high resistivity involves essentially evaporating cadmium and sulfur separately from two independently controlled crucibles onto a substrate which is not viewed directly by the crucibles.

An evaporation system[*] with a 6" all stainless steel pumping system and 18" × 30" pyrex bell jar was installed and modified for the thin film growth. A schematic diagram of the system is shown in

---

Δ Eccofoam, Emerson & Cummings, Inc., Gardena, California
* HVEC Model 618 from High Vacuum Equipment Corp., Hingham, Mass.

Figure 2. Each crucible* was constructed of fused quartz with a central inverted tube for the heater filament. The liquid nitrogen chevron trap at the pumping port served to prevent the sulfur and cadmium vapor from getting into the pumping system.

1 - Quartz Crystal Microbalance and Substrate Holder - In order to measure dynamically the rate of film growth and to monitor the final film thickness, a microbalance was built which records the film thickness on a resonant quartz crystal by recording its change of resonant frequency. The quartz crystal microbalance and substrate holder, shown in Fig. 3, consists of 1) a heater to raise the whole assembly to the temperature (~ 190°C) for optimum CdS crystal growth (Fig. 3b), 2) two identical gold plated quartz oscillator crystals** cut for 9.00 MHz resonant operation mounted inside the substrate holder with one crystal having a face exposed to the vapor (Fig. 3a), 3) a mount for holding the semiconductor substrates to be coated with a CdS film and 4) a remotely operated shutter to expose the substrates and microbalance crystal during vapor growth. The two quartz oscillator crystals are connected to oscillator circuits external to the vacuum system. The oscillator outputs are mixed, and the resulting difference frequency signal is amplified and fed into a frequency meter/ whose output is monitored with a strip chart recorder△. The circuitry involved is shown in Fig. 4.

---

* Obtained from General Electric Company, Willoughby, Ohio
** Reeves Hoffman, Carlisle, Pennsylvania, Type HC-6/U holder
/ General Radio Type 1142-A frequency meter and discriminator
△ Honeywell Electronik 19 two pen recorder

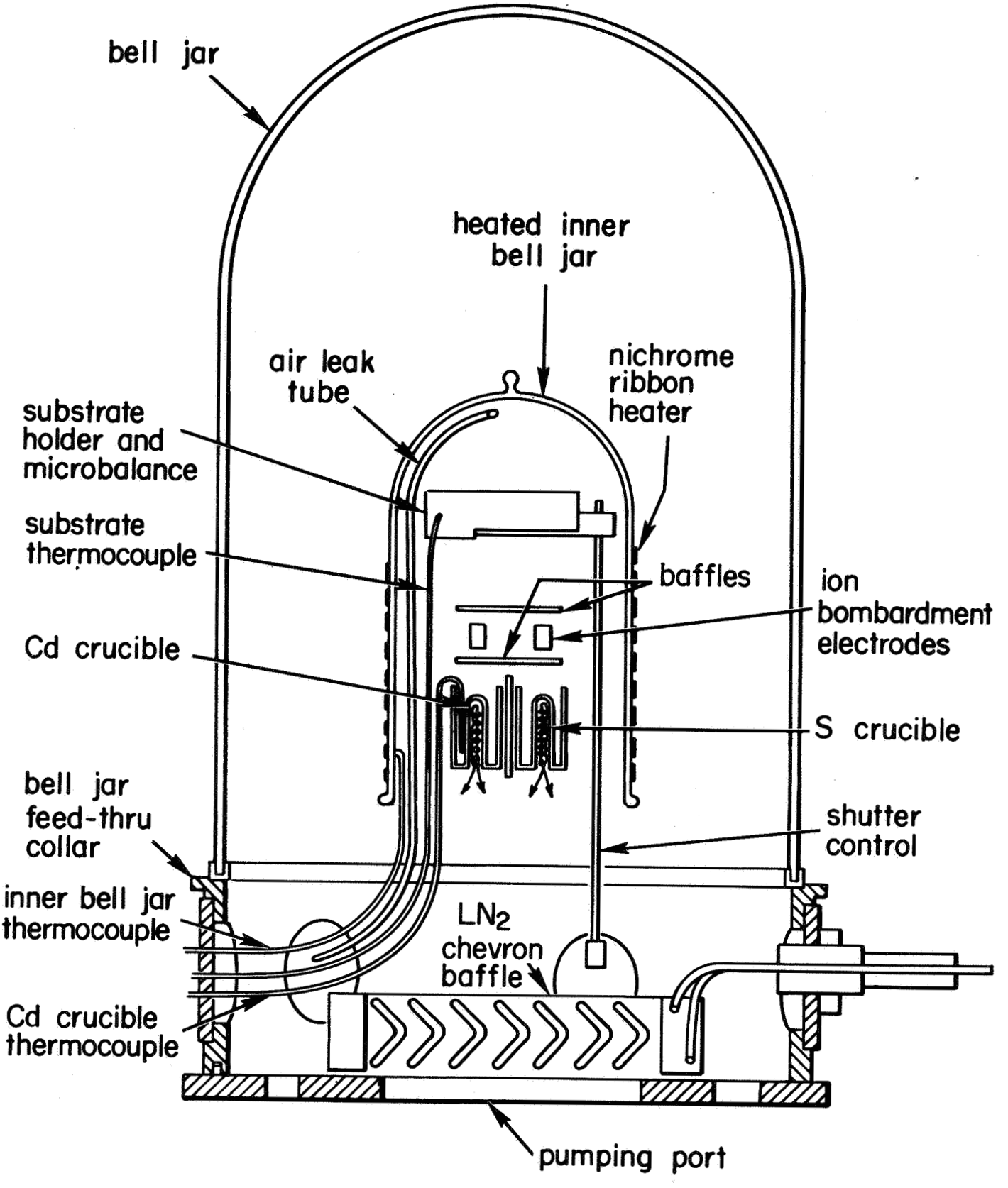

Figure 2 - Schematic diagram of the essential parts of the revised CdS film growth system.

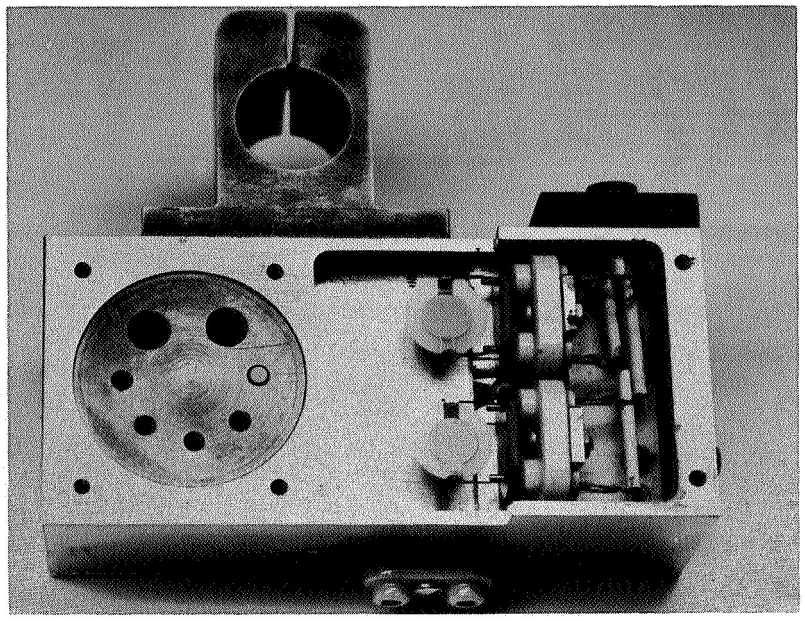

a - Bottom view - Open

This view shows the two quartz oscillator crystals and the exposed substrates.

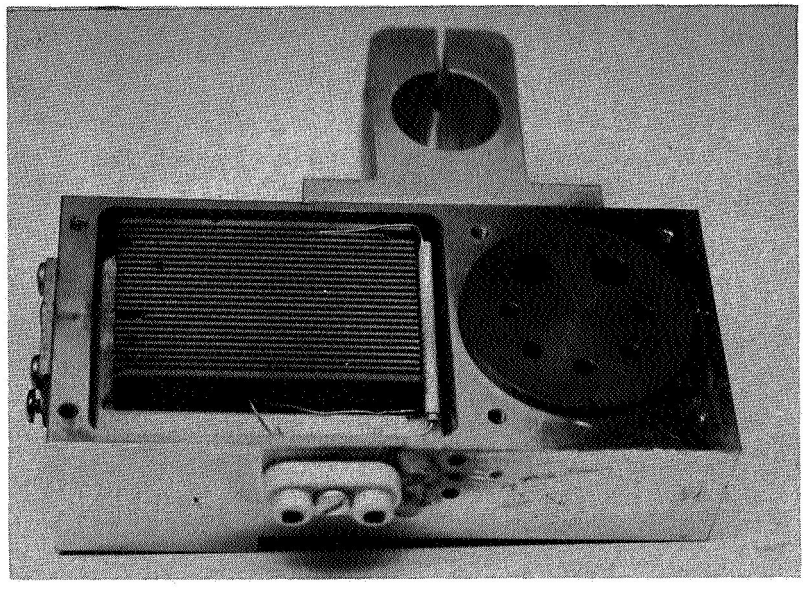

b - Top view - Open

The heater is visible in this view.

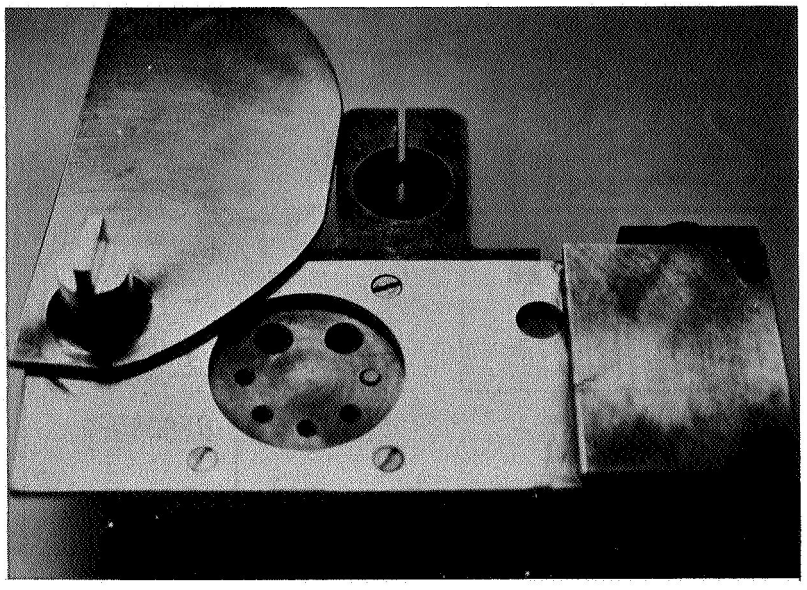

c - Bottom view - Covered

This photo shows the complete unit with shutter open.

Figure 3 - Three views of the substrate holder and micro-balance.

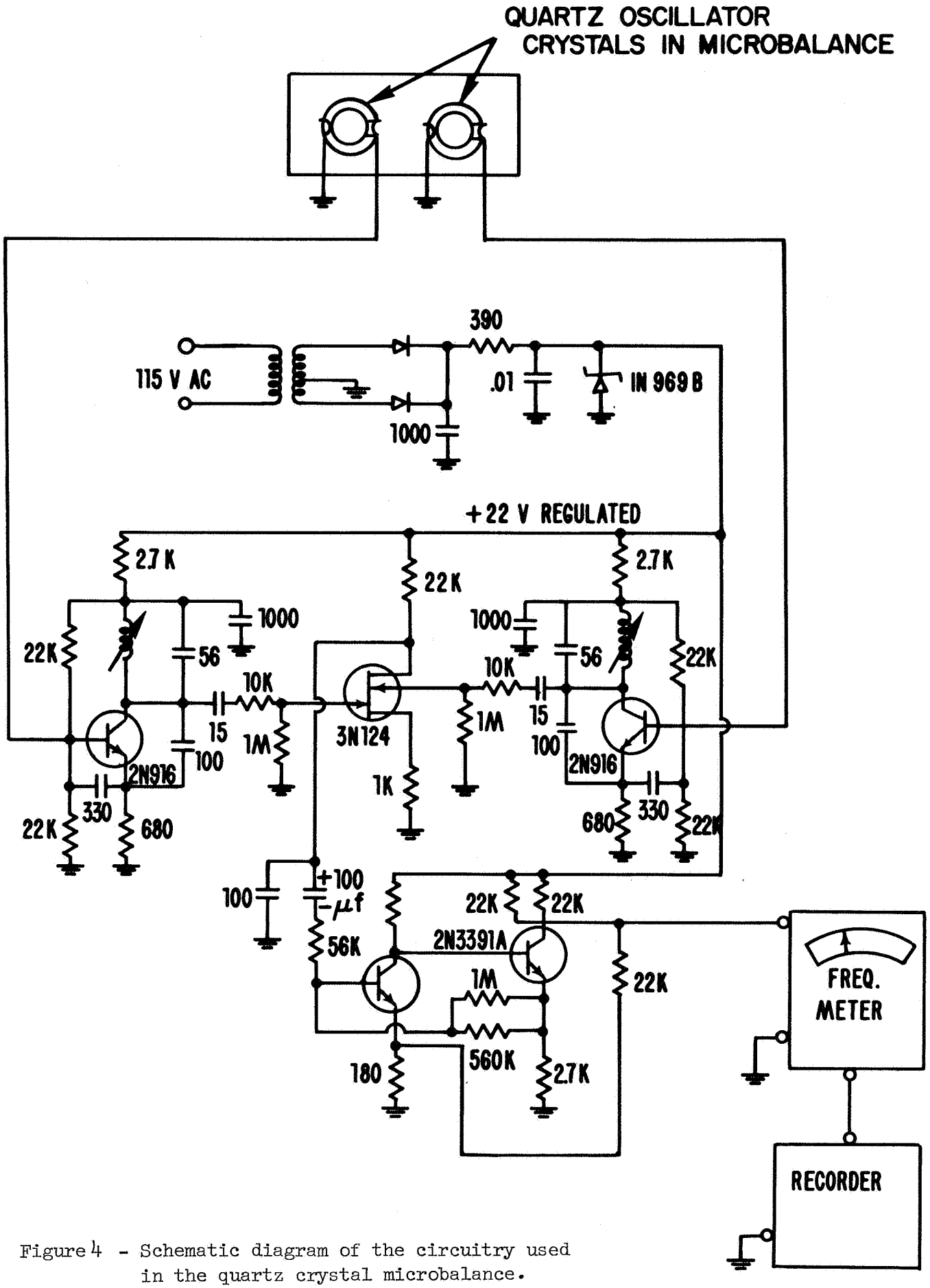

Figure 4 - Schematic diagram of the circuitry used in the quartz crystal microbalance.

The performance of the microbalance was very satisfactory in its stability and its response to the growth of a CdS film. The drift in the difference frequency between the two oscillator crystals was repeatedly less than 0.4 kHz in bringing the substrate holder-microbalance temperature up to 190°C. The effect of opening the shutter (which exposes one microbalance crystal but not the other) was even smaller amounting usually to less than 0.1 kHz. The total frequency change resulting from growth of a 2500 Å CdS film is 23 kHz. The CdS film was cleaned from the microbalance crystal after each evaporation by inserting the crystal for a few seconds in HCl.

Quartz Crystal Microbalance Reading

The quartz crystal microbalance operates by virtue of the change in resonant frequency of the oscillator crystal caused by its increased thickness due to the CdS film. Consider a crystal of thickness S and a film deposited on the surface of thickness dS. Before deposition of the film, the thickness of the crystal is related to the round trip transit time, T, of an acoustic wave from one end to the other and back by the acoustic velocity, v_c, in the crystal

$$S = \frac{v_c T}{2} \quad .$$

Differentiate S with respect to T to obtain the change in thickness corresponding to a change in acoustic transit time

$$dS = \frac{v_c}{2} \quad dT \quad .$$

If the change in thickness is now a thin film with a different acoustic velocity v_t, then it will be written as

$$dS = \frac{v_t}{2} \quad dT \quad .$$

For a resonant crystal the acoustic transit time, T, is precisely the resonant period for a frequency ν

$$T = \frac{1}{\nu} \quad ,$$

thus the change in period corresponding to a change in resonant frequency is

$$dT = -\frac{d\nu}{\nu^2}$$

yielding for a change in thickness

$$dS = -\frac{v_t}{2\nu^2} \quad d\nu$$

For shear waves in CdS $v_t = 1.757 \times 10^5$ cm/sec yielding for our quartz crystals which are resonant at 9.00 MHz,

$$\left(\frac{dS}{d\nu}\right)_{CdS} = 108.5 \text{ Å/KHz}$$

2 - Ion Bombardment Cleaning - An important feature of this method of CdS film growth is that the substrate not be directly exposed to the boiling cadmium and sulfur. A baffle is therefore included in the apparatus between the crucibles and the substrate holder. In order to provide ion-bombardment cleaning of the substrates, this baffle was originally connected to one side of a 2 KV AC potential with the other side of the A.C. potential tied to the substrate holder. Several difficulties arose from this arrangement. The evaporated gold electrode on the microbalance crystal suffered serious damage from cathodic sputtering such as to make the microbalance inoperative.

Furthermore, it was found that a contaminant film tended to build up on the substrate.

Reference to papers by L. Holland[15] on the cleaning of glass in a glow discharge indicated that both these effects are hazards of direct ion-bombardment cleaning as we were attempting to use here. His investigations of the cleaning process demonstrated that an indirect bombardment system was much more suitable especially when contaminants are present in the system. This method involves the use of two electrodes, as shown in Fig. 2, which are physically shielded from the surfaces to be cleaned. Thus there is no danger of high energy electrons in the cathode dark space causing a sputtering of the gold electrode film. This also eliminates the contamination buildup which results from electron bombardment near the fringe of the cathode dark space. The high velocity electrons from the cathode dark space travel outwards from the electrodes away from the substrate where they can do no harm. On the other hand the ions are scattered by colliding with air molecules such that many ions and neutral molecules are scattered onto the substrate where they dislodge loosely adhered contaminants.

After installing such a pair of shielded electrodes as shown in Fig. 2, a number of qualitative tests of the cleaning effectiveness of the ion bombardment were performed. These tests involved ion bombardment of uncleaned, solvent cleaned, and flame cleaned glass surfaces. The flame cleaned surfaces were used as a cleanliness reference in 1) wetting tests, 2) black breath tests, and 3) scratch tests using a flamed glass bead. An ion bombardment run in a carefully cleaned bell jar with no other equipment inside yielded clean surfaces which passed the above three tests. However, the addition of the

remainder of the equipment in the bell jar tended to reduce the effectiveness of the ion bombardment cleaning. This difficulty was eliminated by flushing the bell jar with dry air during the entire ion bombardment. This was done by introducing a regulated leak into the top of the bell jar at a rate just sufficient to maintain a pressure of 50 microns with the diffusion pump wide open. During ion bombardment, the current was maintained for 1/2 hour at 30 ma by adjusting a variac on the primary of a 9 kv, 60 ma neon sign transformer.

3 - Evaporation Procedure - Following the chemical cleaning of the substrate crystal and the microbalance oscillator crystal described in II, and the ion bombardment cleaning discussed in III-2, the system was pumped down to $\sim 10^{-5}$ Torr. The heating of various components of the evaporator system was then begun with temperatures measured by iron-constantin thermocouples. The substrate holder was gradually heated until it reached 190°C where it was held with a temperature controller.* Meanwhile the inner bell jar was heated up to about 130°C while the cadmium was raised to its melting point at 321°C. The sulfur heater was not turned on until some cadmium sulfide deposit started to show on the inner bell jar. Since the melting point of sulfur is 113°, some sulfur was already melting by the time the outer bell jar reached 130°. Aluminum foil was wrapped around the sulfur crucible to prevent the sulfur from heating up too fast and starting to evaporate too soon. The sulfur vapor tended to diffuse throughout the system much more readily than the cadmium, since sulfur simply will not adhere to the warm surfaces. The cadmium, on the other

---

* Temptendor API Instruments Co.

hand, tended to stick much more easily and therefore did not diffuse so readily. The rate of film growth was thus determined largely by the cadmium vapor pressure and the geometry of the system in the paths between the cadmium crucible and the substrate. Some geometries of baffle arrangement which were tried resulted in no film growth whatsoever on the substrates.

When the film growth was seen to progress well on the inner bell jar, the shutter on the substrate holder was opened and the microbalance frequency was monitored. The film growth rate was usually held to less than 5 Å/min.

4 - Evaluation of CdS Films - A glass disc was included in the substrate holder during each evaporation and was used as a comparator between different evaporations. The resistivity of the film was measured in each case and found to be greater than 2×10^8 Ω-cm except in some cases where the Cd vapor pressure had been kept too high. In those cases, the film had an orange color rather than the pale yellow characteristic of the high resistivity films.

a - Examination of Interference Fringes

After removal from the evaporator, the films were all examined in monochromatic 5890 Å Sodium light for interference fringes to check the thickness measurement and evaluate the uniformity of the films.

When monochromatic light impinges on the CdS film some reflects from the surface and some penetrates to the substrate from which it reflects. When the film thickness is a half wavelength the two partial waves are in phase and reinforce each other as they do for any integral multiple half wavelengths. If they are odd multiples of one-quarter wavelength they interfere destructively and produce a dark fringe. The sodium light used has a wavelength in air of $\lambda = 5890$ Å. In CdS with an index of refraction $n = 2.5$ the wavelength is then $\lambda_{CdS} = \lambda/n = 2356$ Å. Thus there will be constructive interference or a bright fringe for each half wavelength or 1178 Å.

Since the substrate is masked during the evaporation and the vapor particles generally approach from angles away from the normal, there is a gradual buildup in film thickness at the edge rather than a sharp cutoff. Thus, from the bright edge where there is no film, one can count the number of bright fringes to the flat central region of the film. This provides a direct measure of the film by multiplying this number of fringes by 1178 Å and estimating the last fraction of a fringe. This can be seen in Fig. 5, which shows a photo of an InSb ingot held in an aluminum ring during the film growth. The outside edge of the aluminum ring was masked by the substrate holder such that the interference fringes could be counted at this point. The microscope enlargement of this edge region shows these fringes very clearly. The picture of the ingot and aluminum ring reveal the extent of nonuniformity. Fig. 5 also shows a microphoto of the inter-

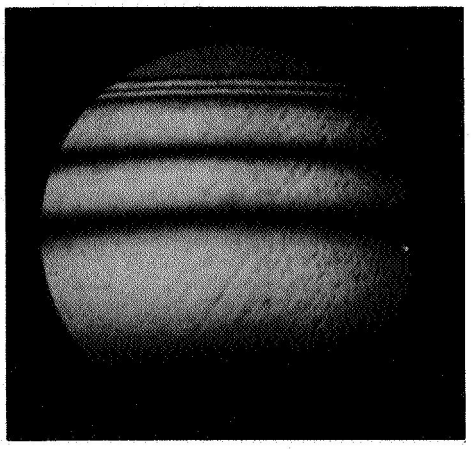

Interference photo of film on aluminum ringholder at edge shown by arrow on middle photo. This shows a thickness at the thickest spot on the ingot of 5 1/2 fringes = 6479 Å
Magnification 12.5 ×

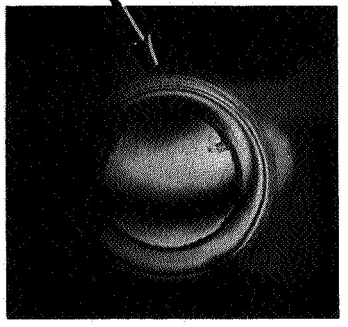

InSb ingot E mounted in aluminum ringholder. This shows a thickness variation of 1-1/4 fringe = 1472 Å over the entire ingot surface. Thus it varies between 6479 Å and 5007 Å from the top to the bottom of the photo. This variation corresponds to 184 Å across a 3 mm diameter rod.

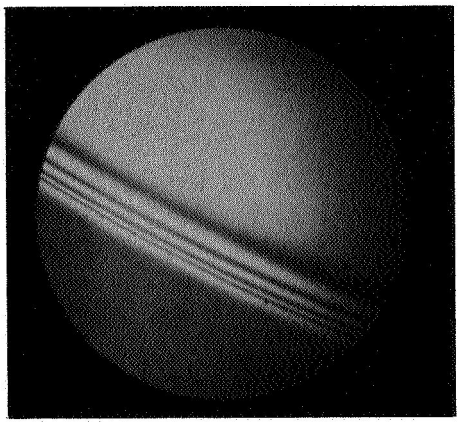

Edge of glass disc showing 4 fringes from the masked edge to the body of the film indicating a thickness of 4 × 1178 Å = 4712 Å
Magnification 25 ×

Figure 5 - Interference photos of CdS films using sodium light (5890 Å). Each fringe represents an integral half wavelength of sodium light in the CdS (index of refraction = 2.5) and therefore represents a film thickness of 5890 Å/(2 × 2.5) = 1178 Å.

ference fringes at the masked edge of a glass disc which was exposed to the Cd and S vapors at the same time. The fringes are much narrower here than those on the aluminum ingot holder since the masking edge was much thinner in this case (.010" instead of .125"). The thinner masking edge causes a much sharper fall off in film thickness.

The film thickness on the microbalance crystal was also examined with the Sodium light. This showed the effects of geometry on the evaporation uniformity. The net result was that the film was not very uniform on this crystal and was only about half as thick as on the other substrates. To within the accuracy allowed by the non-uniformity, the Sodium light determination of the average film thickness on the microbalance crystal agreed well with the measure obtained by the microbalance frequency change during the film growth. This ratio of film thickness on the substrate to that on the microbalance crystal was then used in subsequent evaporations to normalize the microbalance readings.

b - Electron Beam Diffraction Studies of Film Orientation

In order to determine the quality of the films insofar as orientation of the crystal axes is concerned, samples of the films were examined by electron beam diffraction in the RIAS electron microscope.* The 80 kev electron beam is allowed to strike the film with grazing incidence and the reflection diffraction pattern is photographed. Crystal planes which satisfy the Bragg diffraction condition then scatter electrons into spots on the photographic plate. The results for CdS films on two different substrates are shown in Fig. 6. The top

* JEM Inc., Tokyo, Japan serviced by JEOLCO, Inc.(USA), Medford, Mass. 02155

pattern was obtained with the film grown on the glass disc which was exposed to the same evaporation as the InSb substrate from ingot E whose diffraction pattern is also in Fig. 6.

The glass shows diffraction spots characteristic of an oriented film. The spots demonstrate that the c-axis is normal to the film plane, i.e. the spots along a verticle line from the center are spaced exactly right for multiple order reflections from the (002) planes of CdS. The spreading of the spots into lines reveals that the sample is polycrystalline with a variation of about $\pm 5^{\circ}$ in the c-axis orientation.

One would expect a better orientation on a single crystal substrate such as InSb than on glass. However, the diffraction pattern shown in Fig. 6 for the CdS film on InSb showed no spot pattern at all. This indicated that the film was completely amorphous. The most likely reason for this is the surface roughness of the InSb crystal. In order to maintain flatness and parallelism in polishing the InSb ingot surface smoothness had been sacrificed.

Another piece of InSb, E-4, from ingot E was therefore polished to a very high grade finish on a polishing wheel, without regard for flatness and parallelism. Two diffraction patterns of a CdS film, #13, taken with this sample at two orientations rotated 90° from each other in the electron beam are shown in Fig. 7a and 7b. The pictures show the characteristic CdS pattern. However, it is evident in 7b, that the spot pattern seems to be composed of double spots, indicating that the crystallites of CdS have two preferred orientations tilted

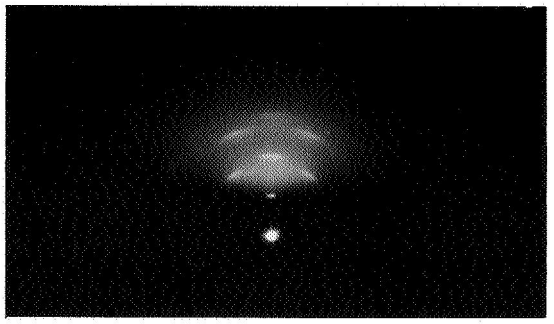

a - Diffraction pattern for CdS film on glass substrate. The locations of the spots are all in good agreement with the tabulated d spacings for hexagonal CdS with the c-axis oriented normal to the film plane. The circumferential spread of the spots indicates a $\pm 5^{\circ}$ variation in the c-axis orientation of the crystallites.

b - Diffraction pattern for Cds film #10 on InSb E5 substrate shown in Figure 8a. The complete lack of clearly defined spots indicates that the film was amorphous.

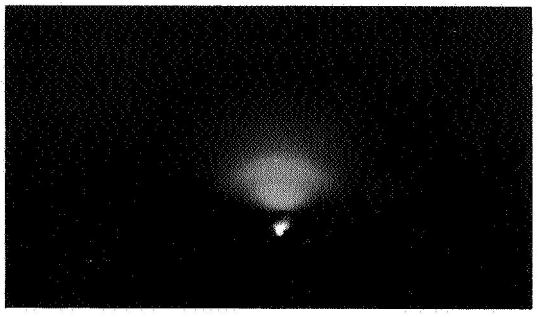

Figure 6 - Reflection electron diffraction patterns for CdS films grown in run #10. Electron energy 80 kv.

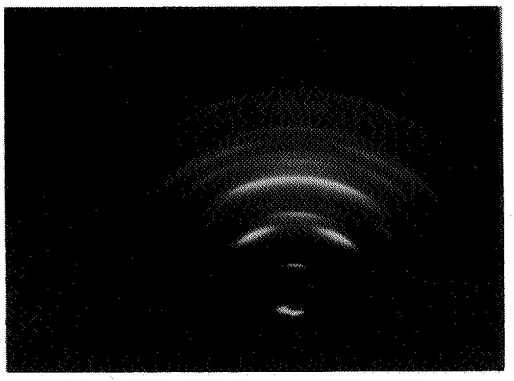

a - Diffraction pattern for CdS film #13 on InSb E-4 with electron beam running parallel to polishing ridges showing single spots.

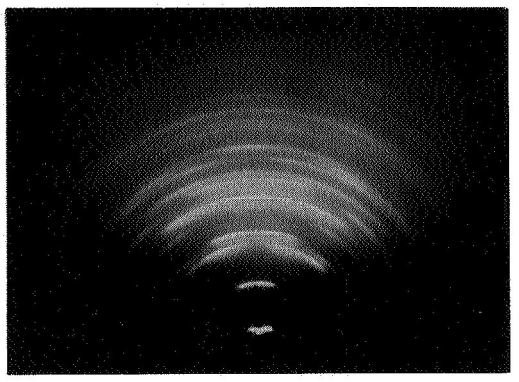

b - Diffraction pattern similar to a- but with double spots caused by electron beam running perpendicular to polishing ridges.

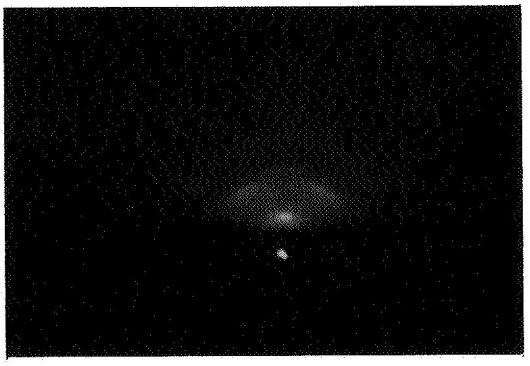

c - Diffraction pattern for CdS film #19 on InSb E7a showing orientation of the film on a polished surface. The duffuseness of the spots indicates small crystallite size. The polished surface is seen in a photomicrograph seen in Figure 8b.

Figure 7 - Reflection electron diffraction patterns for CdS films grown on InSb.

about 20° apart. When viewed at right angles to the direction in which this effect was observed, there was no such doubling of spots (Fig. 7a). Evidently the direction of polishing introduced by the wheel produced enough of a preferred direction of ridges to cause the crystallites to form along both sides of the ridges giving double spots when viewed by the electrons parallel to the ridges and single spots when electrons impinge normal to the ridges.

The remainder of the ingot was then repolished to a higher grade optical finish, while still maintaining reasonable flatness and parallelism, and new CdS films were deposited on the surfaces. The diffraction pattern for this film, #19, is seen in Fig. 7c. The diffuseness of the spots indicates that the crystallites are very small, but there was no evidence of a preferred orientation as evidenced by the wheel polished surface. The surface finishes on the two InSb crystals represented by Fig. 6b and Fig. 7c are shown in Fig. 8. These are photomicrographs taken at a magnification of 300× in the phase contrast microscope[/]. These give some idea of the improvement in surface smoothness required to obtain oriented films.

c - Acoustic Tests of CdS Transducers

In order to test the CdS transducer efficiency some Z-cut quartz rods with the same specifications as the x-cut quartz rods which were used as transducers were obtained[*]. Films from

[/] Leitz-Wetzlar, Germany
[*] Valpey Corporation, Holliston, Massachusetts 01746

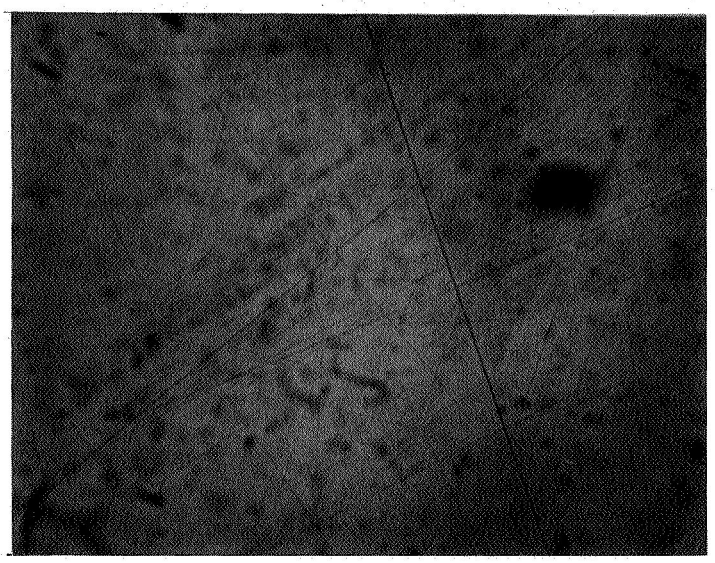

a - InSb E5 before deposition of CdS film. The film on this surface gave diffraction pattern in Figure 6b.

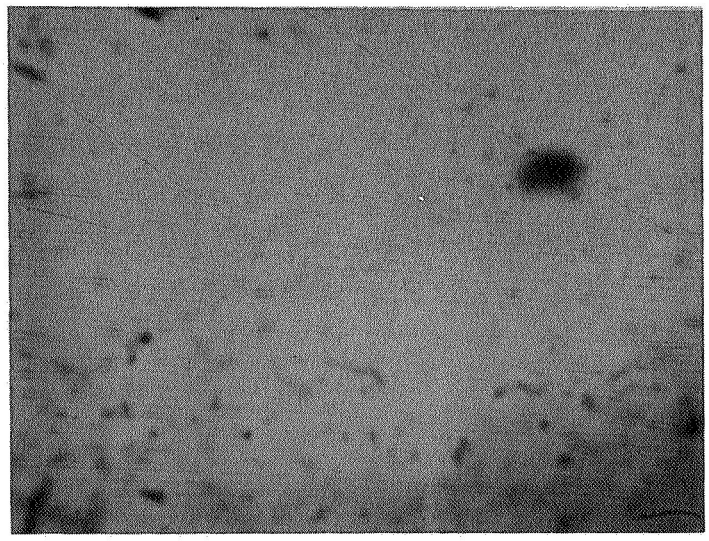

b - InSb E7 before deposition of CdS film. The film on this surface gave diffraction pattern in Figure 7c.

Figure 8 - Photomicrographs of polished surfaces on InSb crystals E5 and E7 taken with phase contrast microscope at magnification 300x, showing the difference in the quality of the polish required to get oriented CdS films.

evaporation #13 on two z-cut quartz crystals were tested for transducer efficiency in the microwave acoustics system. Since the z-axis of quartz is not piezoelectric one does not get any transducer action on the part of the quartz, only the CdS film. The first acoustic echoes for both these rods were about 42 db above the noise which is about 10 db less efficient than the better x-cut quartz transducers.

Films were deposited on crystals from ingot D in which acoustic waves had previously been seen with the use of x-cut quartz transducers (Section V) and also on E-5 as discussed above in Section III-4-b. No acoustic echoes were seen with the use of these films which were found subsequently to be amorphous by the electron diffraction tests. The film, #19, deposited on InSb-E7a which was shown in III-4-b to have crystalline structure was also unsuccessful in producing observable acoustic echoes. Similarly, the same film on rods E7f, E7h and E7i cut from the same piece resulted in no echoes. Subsequent tests using an x-cut quartz transducer (Section V) on InSb-E7i (which was cut from the same piece as E7a) was successful in producing echoes 17 db above the noise. Thus, if the 10 db loss in efficiency which was observed for the CdS films on z-cut quartz applies to the InSb, the echoes for E7a should have been visible 7 db above the noise. However there are two factors which would tend to reduce this efficiency further with the InSb. The first is the small crystallite size observed (Section III-4-b) for the CdS film on InSb-E7a. The other factor is a reduction to 55% of its original value in the Q of the microwave cavity which occurs when InSb rods are inserted instead of quartz rods. This has the effect of reducing the amplitude of the microwave electric field across the gap where the rod is inserted and thus reducing the transduction efficiency.

IV. THEORY OF ELECTRON-PHONON INTERACTIONS

The attenuation of acoustic waves by interaction with conduction electrons in single valley semiconductors was treated for a number of circumstances by Mikoshiba[2] using the approach developed by Pippard[16] for monovalent metals. He calculated the acoustic attenuation, α, and the inverse effect, the acoustoelectric potential, F, for both $q\ell > 1$ and $q\ell < 1$ where ℓ is the electron mean free path and $q = 2\pi/\lambda$ is the acoustic wave number. The mean free path is derived from $\ell = v_e \tau$ where v_e is the mean electron thermal velocity and $\tau = (m/e)\,\mu$ is the mean time between electron collisions. (μ is the electron mobility.) If the electron density is great enough for degenerate statistics to apply then the mean velocity is simply the Fermi velocity. On the other hand, v_e becomes the kinetic velocity associated with the mean Boltzman energy if the electrons are isolated enough to obey non-degenerate statistics. Our experiments with high purity InSb in the 9 GHz range are principally in the region of non-degenerate statistics and with $q\ell > 1$. The acoustoelectric effect is observed as a voltage pulse across the semiconductor which occurs as a result of the passage of the acoustic wave. The acoustoelectric potential and the attenuation coefficient are related by

$$\frac{\alpha}{F} = \frac{Ne\, v_s}{\Gamma} \quad , \tag{1}$$

where

N = carrier electron concentration

v_s = velocity of sound

and $\Gamma \equiv \rho|u|^2 v_s/2$ is the acoustic energy flow density. It therefore represents the acoustic power per unit area fed into the crystal by the transducer.

The expressions for attenuation, α, can be written in terms of a temperature dependent term A(T) and of a temperature independent coupling coefficient K which involves a piezoelectric coupling coefficient K_p and a deformation potential coefficient K_d.

Thus

$$\alpha = K^2 A(T) \tag{2}$$

where

$$K^2 = K_p^{\,2} + K_d^{\,2} \qquad K_p^{\,2} = \frac{e_p^{\,2}}{\epsilon c} \qquad K_d^{\,2} = \frac{\epsilon\, q^2\, C_l^{\,2}}{\epsilon^2 c} \tag{3}$$

In the (100) direction in the III-V cubic compounds $K_p^{\,2} = 0$ and measurements thus yield $K_d^{\,2}$. In the (111) direction, both $K_p^{\,2}$ and $K_d^{\,2}$ contribute. In these experiments the absolute value of α is difficult to measure accurately because of uncertainties in transducer efficiency and because of other losses besides electronic attenuation. However, the value of K^2 can be obtained from the slope of α vs. A(T) in the measurements and the absolute value of α obtained from the intercept.

An independent and valuable determination of K^2 can be obtained by taking into account the effect of an electron drift velocity on the attenuation. The theory for this circumstance derived by Spector[1] for both $q\ell > 1$ and $q\ell < 1$ and by White[6] for $q\ell < 1$ has the same basic form but includes the term $\gamma = 1-(\mu E)/v_s$ which embodies the electric field dependence of the attenuation.

These theories yield

$$\alpha = K^2 A(T,\gamma); \tag{4}$$

where

$$A_<(T,\gamma) = \frac{\omega_c}{2v_s \left[\gamma + \frac{1}{\gamma}\left(\frac{\omega_c}{\omega} + \frac{\omega}{\omega_D}\right)^2\right]} \qquad \text{for } q\ell < 1 \tag{5}$$

and

$$A_>(T,\gamma) = \frac{3\pi\omega\gamma\omega_c}{4v_e\omega_D\left(\frac{\omega_c}{\omega} + \frac{\omega}{\omega_D}\right)^2} \qquad \text{for } q\ell > 1 \tag{6}$$

where

e_p = piezoelectric constant in the direction of acoustic propagation

C = elastic constant for the relevant direction of acoustic propagation and polarization

ω_c = $\frac{\sigma}{\epsilon}$ = dielectric relaxation frequency

σ = electrical conductivity

ϵ = dielectric permetivity

γ = $1 - \frac{\mu E}{v_s}$

μ = electron mobility

E = applied electric field

ω = acoustic wave circular frequency

ω_D = v_s^2/D = diffusion frequency

D = diffusion constant = $\frac{\mu kT}{e}$ (by Einstein relation)

k = Boltzman constant

T = electron temperature

e = electronic charge

v_e = mean electron velocity (discussed above)

The expressions for $A(T,\gamma)$ reduce to those for $A(T)$ derived by Mikoshiba[2] when $\gamma = 1$ i.e. when the applied electric field is zero. The values of $A(T)$ calculated for InSb Ingot E for which we measured the conductivity and Hall coefficient are shown in Figure 9. This sample had a net carrier concentration of $N = 1.1 \times 10^{14}$ cm^{-3} derived from our Hall coefficient measurement.

The equivalence of White's[6] equation for $A(T,\gamma)$ to Spector's[1] expression for the corresponding case of $q\ell < 1$ is not obvious since Spector's equation appears in the form

$$\alpha_{p<} = \frac{q^2 \tau \gamma (\omega/\omega_p)^2 d_{xz}^2}{12 \pi \rho v_s \left\{\gamma^2 \left(\frac{\omega}{\omega_p}\right)^4 + (\omega\tau)^2 \left[1+\frac{1}{3}\left(\frac{v_F}{v_s}\right)^2\left(\frac{\omega}{\omega_p}\right)^2\right]^2\right\}} \qquad (7)$$

where

ω_p = electron plasma frequency $= \left(\frac{Ne^2}{m\epsilon}\right)^{1/2}$

d_{xz} = piezoelectric constant

ρ = mass density of crystal

v_F = Fermi velocity of conduction electrons

We can try to cast equation (7) into the form of (5), which is basically White's form, in order to compare the predictions of the two theories for the same applicability ($q\ell < 1$ and piezoelectric coupling). However, we must note that White derived equation (5) using non-degenerate electron statistics whereas Spector derived (7) using degenerate Fermi statistics.

Note that: $q = \omega/v_s$, and $\rho v_s^2 = c$.

We can make these substitutions in (7) and divide numerator and

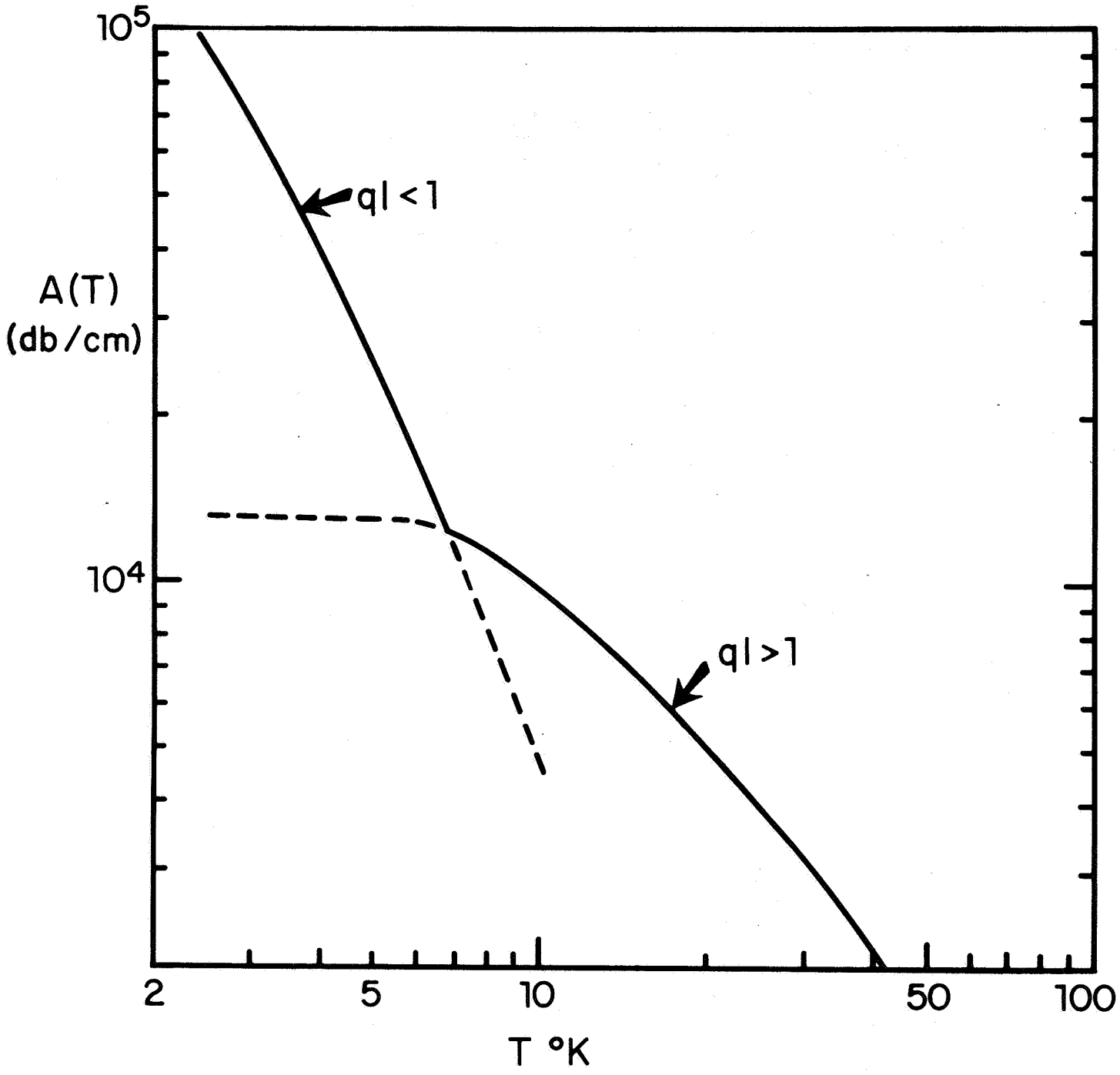

Figure 9 - Calculated dependence of A(T) on temperature for $q\ell < 1$ and $q\ell > 1$.

denominator by $(\omega/\omega_p)^4$ yielding:

$$\alpha_{p<} = \frac{\tau\,\omega_p^2\,d_{xz}^2}{12\,\pi\,c\,v_s}\left[\gamma + \frac{1}{\gamma}\left(\frac{\tau\,\omega_p^2}{\omega} + \frac{\omega\,\tau}{3}\,\frac{v_F^2}{v_s^2}\right)^2\right]^{-1} \qquad (8)$$

Noting the definition of the dielectric relaxation frequency in (5) we see that:

$$\omega_c = \frac{\sigma}{\epsilon} = \frac{Ne\mu}{\epsilon} \quad ,$$

we saw that the electron mobility is related to the mean collision time, τ, by

$$\mu = \frac{e}{m}\,\tau \quad .$$

Thus

$$\omega_c = \frac{Ne^2}{m\epsilon}\,\tau = \omega_p^2\,\tau \quad .$$

Now equation (8) becomes

$$\alpha_{p<} = \frac{d_{xz}^2}{6\,\pi\,c}\,\frac{\omega_c}{2v_s}\left[\gamma + \frac{1}{\gamma}\left(\frac{\omega_c}{\omega} + \frac{\omega\tau}{3}\,\frac{v_F^2}{v_s^2}\right)^2\right]^{-1} \qquad (9)$$

This looks very much like the form of (5) where the piezoelectric coupling constant would be

$$K_p = \left(\frac{d_{xz}^2}{6\,\pi\,c}\right)^{1/2} \quad .$$

It is difficult to relate this expression exactly to the coupling coefficient

$$K_p = \left(\frac{e_p^2}{\epsilon c}\right)^{1/2} \quad ,$$

since Spector uses a rather unconventional piezoelectric constant. If we presume that the two coupling coefficients are equivalent, we can now

examine the equivalence of the two theories. The two expressions (5) and (9) are now identical except for the last term in the denominator of both, viz

$$\frac{\omega}{\omega_d} \text{ and } \frac{\omega\tau}{3} \frac{v_F^2}{v_s^2} \quad \text{respectively.}$$

According to the definition of ω_d, we see that

$$\omega_d = \frac{v_s^2 e}{\mu kT} = \frac{m v_s^2}{\tau kT} .$$

Thus the two last terms become

$$\frac{\omega\tau}{v_s^2} \frac{kT}{m} \text{ and } \frac{\omega\tau}{v_s^2} \frac{v_F^2}{3} ,$$

and it becomes evident in comparing these terms from the two theories that if we equate the Fermi energy $= \frac{1}{2} m v_F^2$ to the Boltzman mean energy $= 3/2$ kT then these two terms are identical. This comparison demonstrates where the difference between degenerate and non-degenerate statistics appears in the two theories. Spector's equation for deformation potential coupling in the region of $q\ell < 1$ similarly reduces to equation (5) except for a factor of $2/3$. When $\gamma = 1$ Mikoshiba's result agrees exactly with Spector's, rather than White's. Equation (6) was obtained from Spector's theory by using the same transformations that were involved in going from equation (7) to equation (5).

The expressions for $A(T,\gamma)$ are antisymmetric about $\gamma = 0$ yielding a negative attenuation, or gain, when $\gamma < 0$. The interpretation, however, is not quite so simple as might be presumed from the form of the theoretical expressions, since the mobility μ is a function of the electric field E which can be seen from our measurements of μ vs. E in Fig. 10. (These are discussed in Section VI.) Moreover, the dependence of μ on E is due to the rise in electron temperature produced by the electric field. Therefore the electric field dependence of $A(T,\gamma)$ has to include the electron temperature change produced by the field. The electron temperature dependence of the mobility is obtained from measurements of mobility as a function of lattice temperature as discussed in Section VI and shown in Figure 11. The dependence of $A(T,\gamma)$ on electric field is thus calculated using this measured dependence of mobility and electron temperature on electric field, yielding the attenuation and amplification curve shown in Figure 12.

V. PHONON PROPAGATION IN InSb

1 - InSb - Cl, 0.318 cm long - It was indicated in Section IV that one can obtain a measure of the coupling coefficient K^2 by measuring the slope of $A(T)$ vs. α and that the absolute attenuation can be obtained from the intercept. From the data obtained in the previous work[10] with InSb-Cl, it was evident that a decrease in acoustic attenuation accompanied a rise in temperature from 4.2° to 14.5°K. Because of the large interference effects, the change in attenuation per unit length obtained from these measurements varied greatly from echo to echo such that the increase in amplitude was as high as

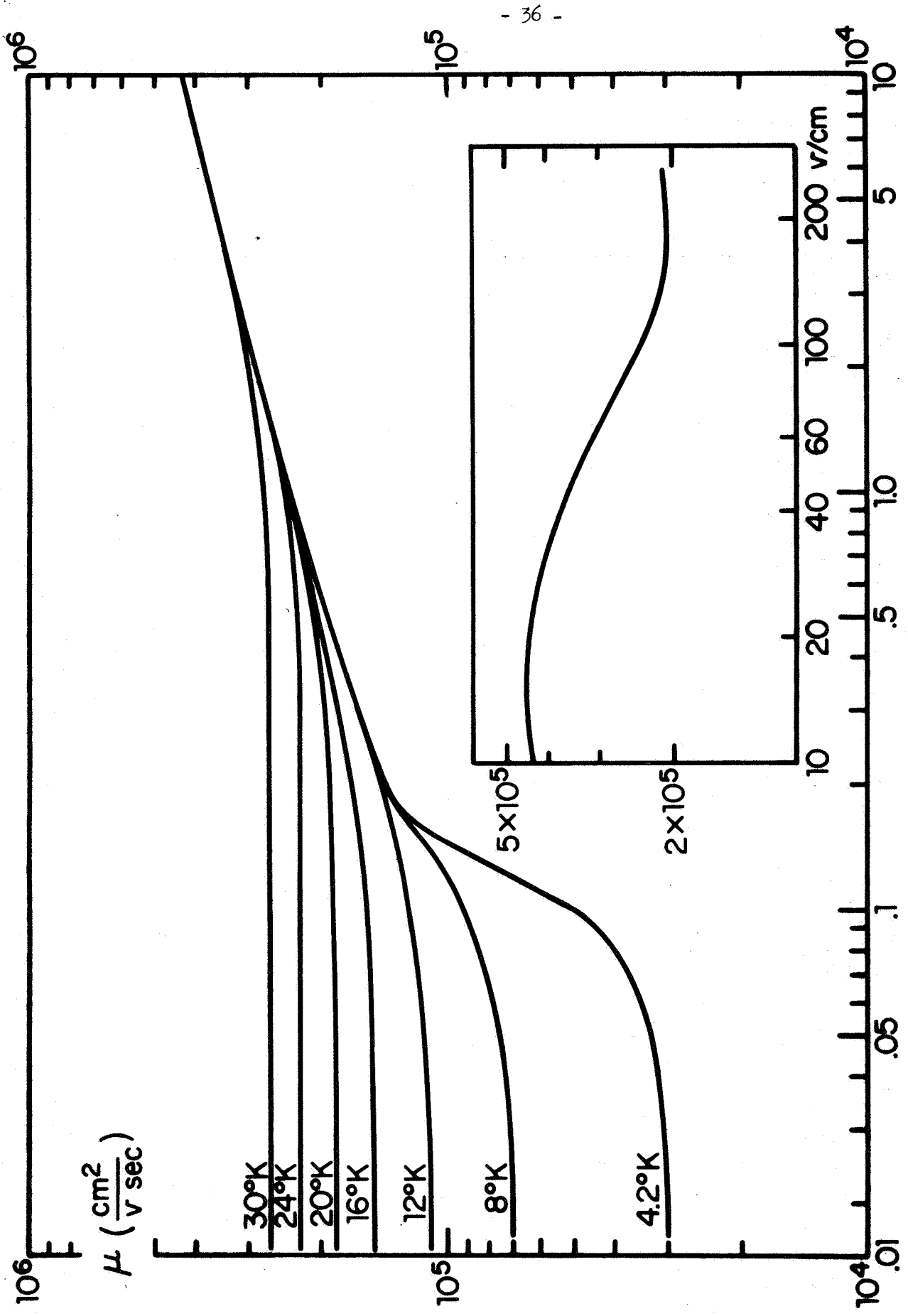

Figure 10 - Measured values of mobility dependence on electric field at different lattice temperatures for InSb with N = 10^{14} cm-3.

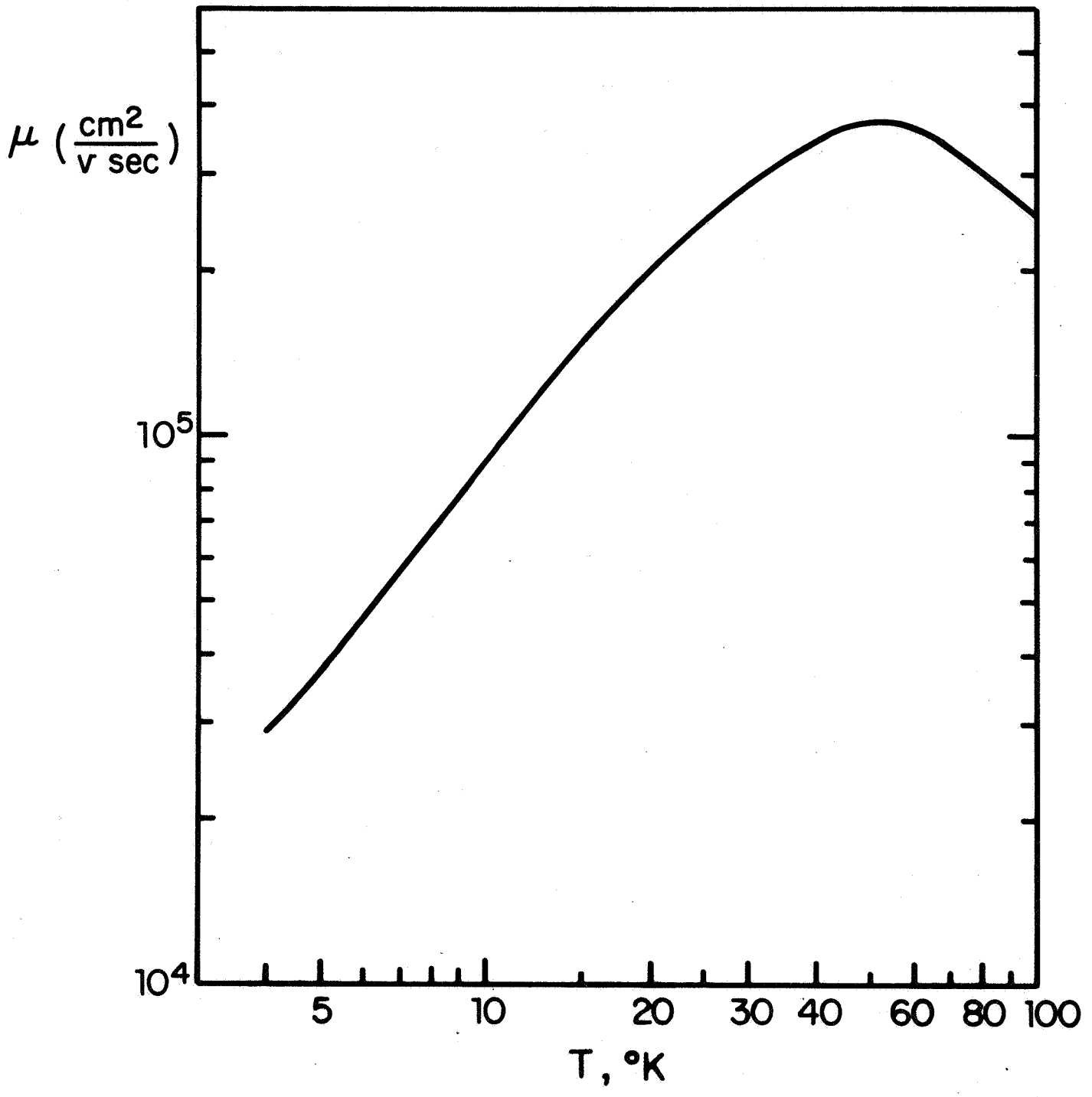

Figure 11 - Measured values of mobility dependence on lattice temperature for InSb with N = $10^{14}cm^{-3}$.

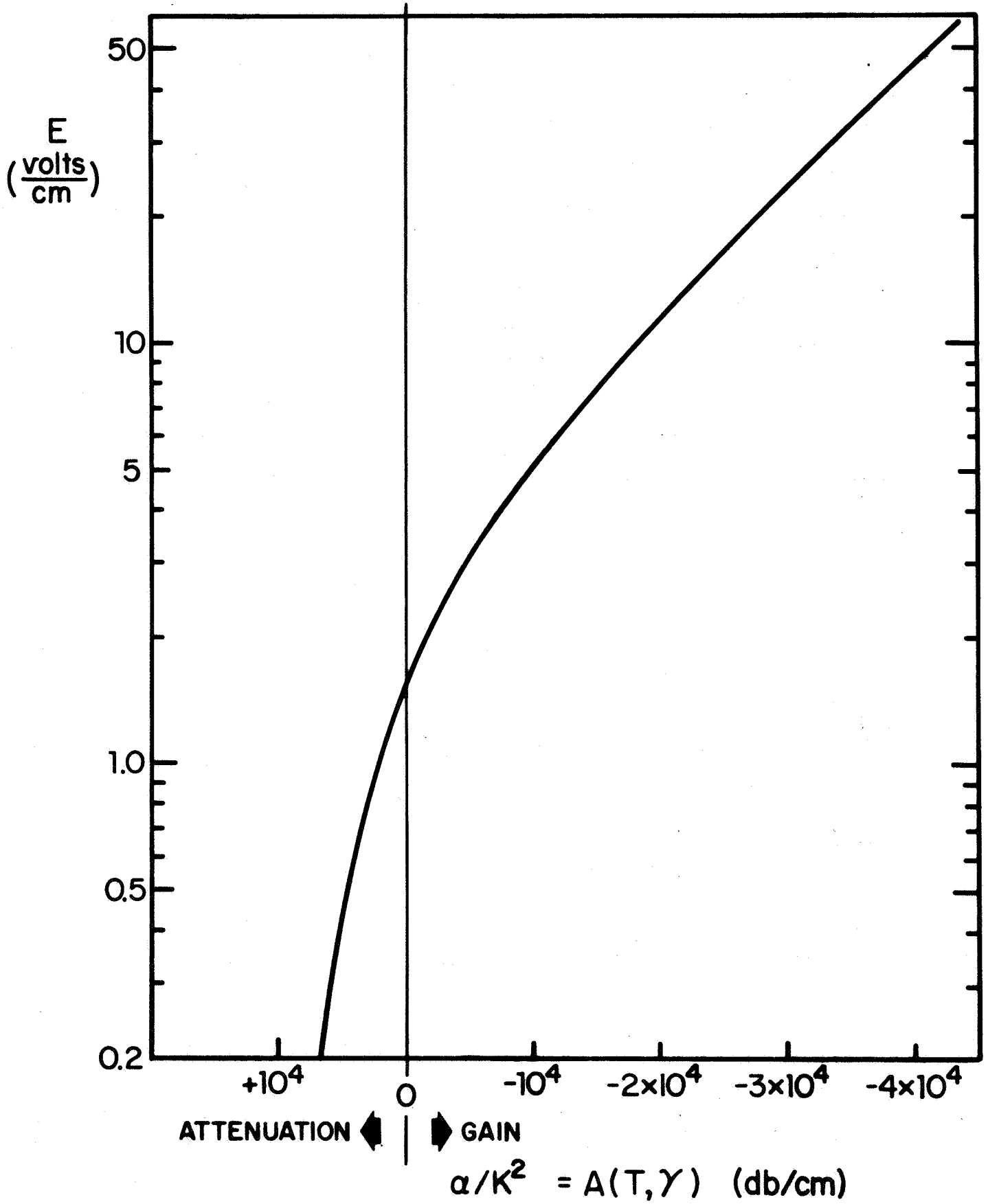

Figure 12 - Calculated dependence of $A(T, \gamma)$ on electric field for $q\ell > 1$ for the sample whose mobility measurements are given in Figures 10 and 11.

3 db/cm in going from 4.2° to 14.5°K. However, since there were six echoes representing one acoustic round trip through the InSb and six more echoes representing two round trips, it seems reasonable to average the measured changes in order to average out the interference effects. The results of this procedure are shown in Fig. 13 with α_M being the measured decrease in attenuation relative to 4.2°K. We note from Fig. 9 that the transition from validity of the $q\ell > 1$ theory to the $q\ell < 1$ theory occurs in the vicinity of 7°K. Thus one does not expect the values of A(T) to be reliable in this region. We therefore take the measurements at 4.2°K and 14.5°K as points where the theories are valid to determine the slope and intercept of α vs. A(T). We get the results that the absolute attenuation at 4.2°K is $\alpha_o = 12$ db/cm and the coupling coefficient is $K^2 = 3.3 \times 10^{-4}$.

It is interesting to compare this value of α_o with upper limit values of α_o obtained from absolute efficiency determinations of the acoustic transducer. From the results with InSb-Cl, the largest echo was (1-3). This represents two passages through the InSb-quartz bond and two reflections from the bond. The power loss upon transmission was estimated at 1 db and the power loss on reflection at 7 db. (The acoustic match is such as to give ~ 80% transmission and ~ 20% reflection). This echo had a measured amplitude of -43 dbm as compared to -18 dbm for the first echo from the quartz transducer, Qi6, before having the InSb attached. Thus of the 25 db (43 dbm-18 dbm = 25 db) reduction in amplitude seen in echo (1-3), 1 + 1 + 7 + 7 = 16 db is caused by power losses at the various transmissions and reflections

$$\alpha = K^2 A(T) \qquad \text{but } \alpha = \alpha_M + \alpha_0$$

$$\alpha_M = \alpha - \alpha_0 = K^2 A(T) - \alpha_0$$

$$\frac{d\alpha_M}{dA(T)} = K^2$$

$$\alpha_0 = 12 \text{ db/cm}$$

$$K^2 = \frac{12 \text{ db/cm}}{36 \times 10^3 \text{ db/cm}} = 3.3 \times 10^{-4}$$

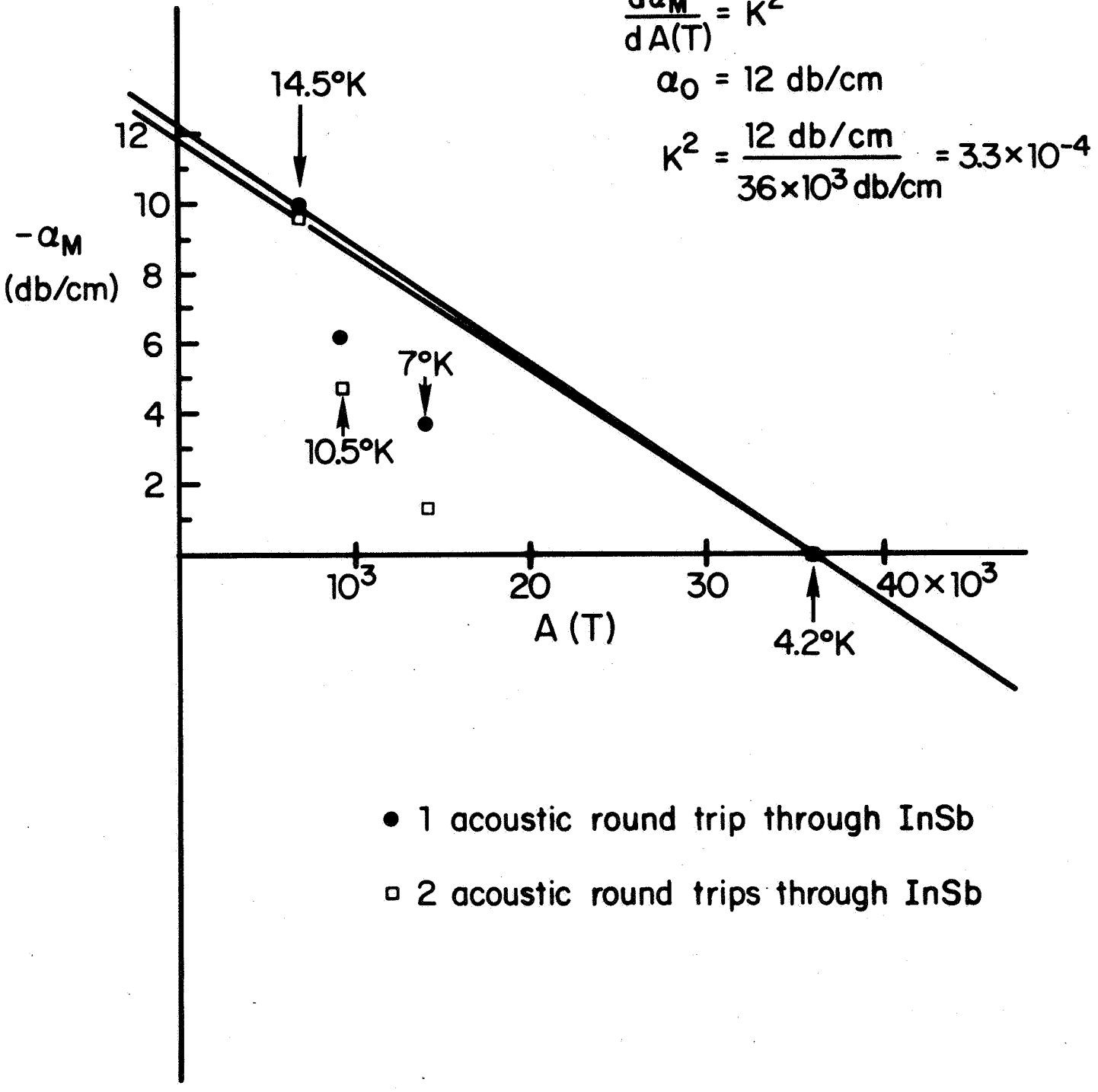

Figure 13 - Determination of the coupling coefficient K^2 and the absolute attenuation α_o from the temperature variation of measured attenuation.

leaving 9 db attenuation in the round trip through the InSb. Since this crystal was 0.318 cm long, this represents a value of 14.2 db/cm for an upper limit to α_o. This is not too far from the value of 12 db/cm deduced from the A(T) vs. α intercept.

The value of coupling coefficient, K^2, deduced from the slope determination agrees exactly with a value of $K^2 = 3.3 \times 10^{-4}$ obtained by Nill[17] by fitting magnetoacoustic attenuation data at 9 GHz. However, the slope of the attenuation versus temperature which we obtained is considerably greater than that shown by Nill in the same work. He saw a change of only 1.3 db/cm between 4.2°K and 14.5°K.

2 - InSb - D3b, -D3e, C2b - In order to obtain a better idea of the consistency of results for the absolute attenuation of acoustic waves in InSb a number of other short crystals were attached to quartz transducers similar to InSb-C1 discussed above. Short crystals have the advantage that the acoustic path is short and so echoes are still measureable even with a large attenuation. However such short crystals cannot have electrical contacts attached for pulsing with an electric field since the contacts would be too close together for meaningful results. Moreover the acoustic transit time is so short that, if a CdS film transducer is used, the first echo returns before the receiver saturation from the magnetron pulse has recovered. It is therefore necessary to use as a buffer, a quartz rod transducer as in the previous experiment.

Thus a disc 0.455" in diameter and 0.22" thick from ingot D was polished as described in Section II. It was glued to a 0.25" diameter x-cut quartz transducer and examined for echoes. None were

observed from the InSb and after removing the assembly from the cryostat, the crystals fell apart with a piece of InSb having broken away from the crystal and remained glued to the quartz.

The remaining portion of the InSb crystal was then ground down and repolished, this time with a thickness of 0.144" remaining. One of the smaller diameter (0.118") quartz transducers was glued to the center of this crystal and tested. Again 5 reflections from the quartz - InSb interface were visible but none from the far end of the InSb. This quartz crystal was then separated by dissolving the glue and it was found that the InSb had developed a crack all around where the quartz had been attached. It thus appeared as though such configurations of dissimilar diameters produced too great a stress on the InSb.

A rod 0.118" in diameter was then cut from between the edge and the center of this disc with the ultrasonic cutter. This rod, InSb-D3b, was glued to the same quartz crystal, Qi7, used in the previous test and examined for echoes. This time reflections from the InSb were not at all as large as those observed with InSb-C1. Ten reflections from the InSb were observed in this crystal whose echo pattern is shown in Figure 14a. This picture shows the first five quartz reflections (0-1, 0-2, 0-3 etc.) and the first five InSb reflections (1-1, 1-2, 1-3 etc.). The largest InSb reflection (1-3) was 12 db above noise. A second 0.118" diameter piece (InSb-D3c) was cut from the disc and mounted on a quartz transducer and tested. No echoes were seen from the InSb in this case, only the reflections from the quartz-InSb interface. A third similar piece (InSb-D3d) was

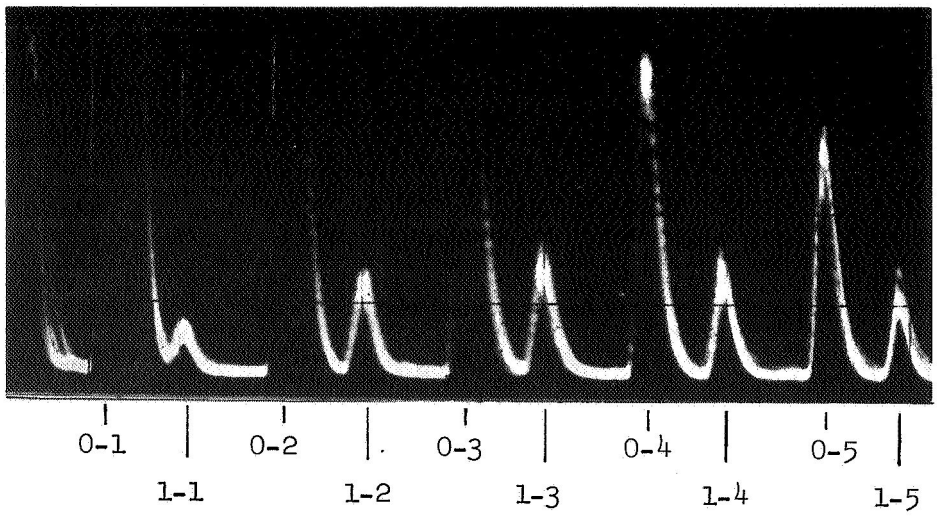

a - InSb -D3b on Transducer Qi7

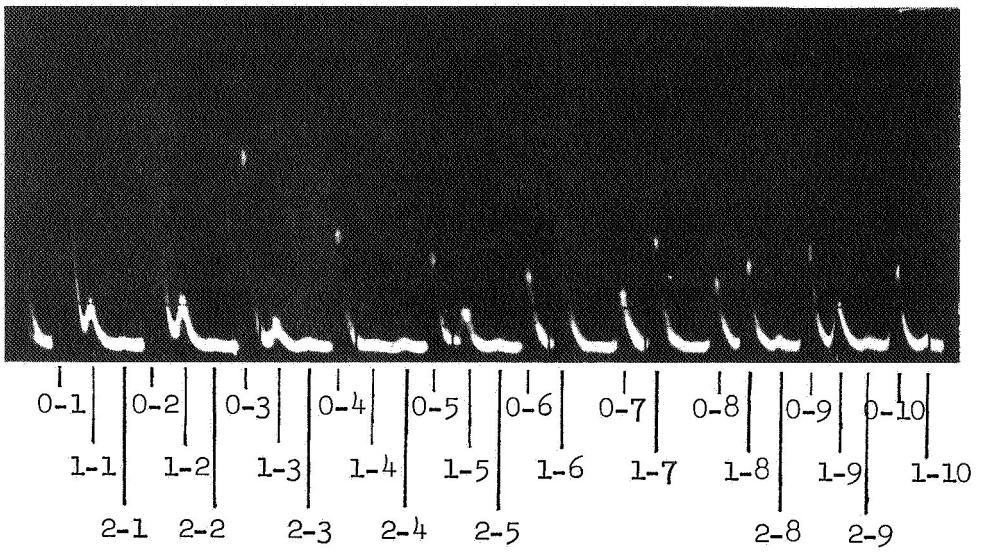

b - InSb -D3e on Transducer Qi8

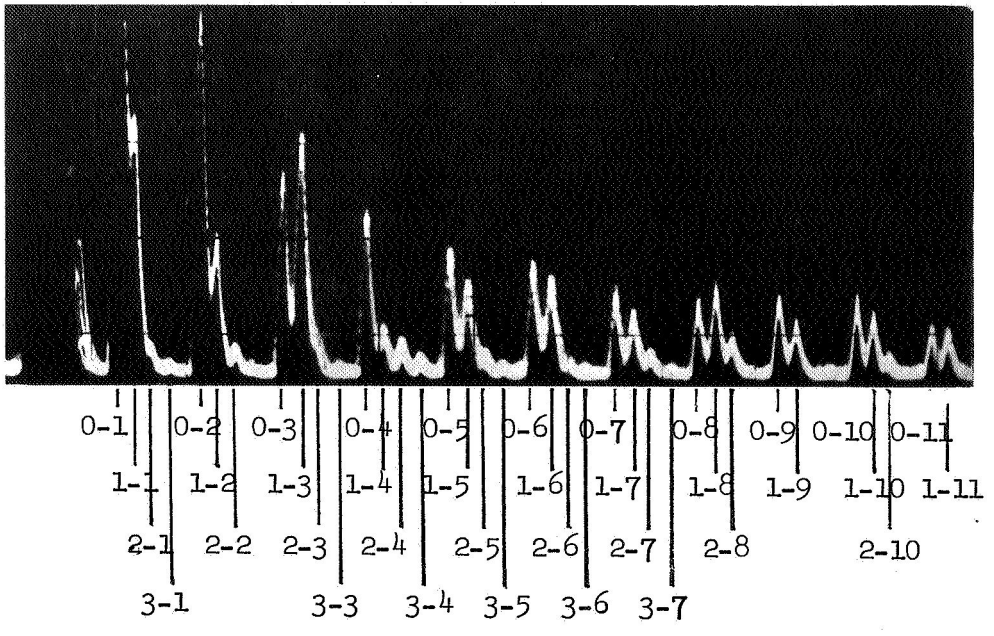

c - InSb -C2b on Transducer Qi4

Figure 14 - Acoustic echoes at 9.3 GHz for three InSb samples attached to quartz transducers rods. The symbols on the lines pointing to the various echoes denote the number of round trips thru InSb and thru quartz, e.g. 1-2 denotes one round trip thru InSb and two thru quartz.

cut and tested with still no InSb reflections. Finally a fourth piece (InSb-D3e) was cut and glued to the quartz transducer with the results shown in Figure 14b. In this case, we see again reflections from the InSb including multiple reflections such as 2-3, 2-4 and 2-5. Here the largest InSb reflection is 1-6 which is 20 db above noise.

The difficulty in getting a reliable bond between the quartz transducer and the InSb crystal seems to be the predominant factor involved in the failure to get phonon propagation in two out of the four cases discussed above. Subsequent microscope examination of the bond in the case of InSb-D3d showed a breaking away of the bond over most of the surface with three optical interference fringes in evidence.

A final attempt was made to obtain rods from ingot C by polishing a thin disc which still remained. Due to the thinness of the disc it had to be mounted on a backing glass during polishing to prevent flexing. Two rods 0.118" diameter and 0.074" long (InSb-C2a, C2b) were cut from this, glued to quartz transducers (Qi8 and Qi4 respectively) and tested for echoes. No InSb echoes were seen from C2a but they were seen with C2b. The acoustic echoes from this assembly are seen in Fig. 14c where reflections representing two and even three InSb round trips are seen. The largest InSb reflection here is (1-3) which is 26 db above noise.

The temperature of all these crystals was varied from $4.2^{\circ}K$ to $20^{\circ}K$ and no change in amplitude was observed in the echoes as with InSb-C1 nor was there any evidence of the frequency shift effect seen

with InSb-Cl. The bonding of crystals here seemed to be somewhat unreliable since echoes were visible from only half of the attempts and those that were visible resulted in very high apparent absolute attenuation. It was after these tests that the method for gluing crystals described in Section II was initiated.

3 - InSb E7i 0.825 cm long - After unsuccessful attempts at seeing echoes with the use of CdS films on InSb E7f, E7b, and E7i the latter was glued onto quartz transducer QV6 which is 1.712 cm long corresponding to a 6.0 μsec acoustic round trip. The InSb-E7i length corresponds to a 4.4 μsec round trip. For the first time acoustic reflections were visible in an InSb rod which is long enough to attach electrical contacts. The largest InSb echo (1-1) was 63 dbm with a quartz transducer that yielded a first echo of 31 dbm before attaching the InSb. Thus the upper limit to the absolute attenuation seen here is 18.2 db/cm.

The current and voltage leads described in Section II were then attached to the crystal and pulses from a 50Ω pulse generator* were fed through a 7:1 turn pulse transformer to give an impedence transformation of 49:1. The size of a typical current passed through the InSb using this generator is 0.6 amps, corresponding to a field across the crystal of about 1.2 volts/cm. which corresponds to a drift velocity of 2.7×10^5 cm/sec. This is about 0.7 times the sonic velocity in the (111) direction in InSb. An increase in amplitude in the echo (1-1) and in other echoes passing through the InSb has apparently been achieved when the applied pulse was coincident with the time that the

---

* Hewlett Packard Model 212A

acoustic wave is traversing the InSb. A high current pulse generator* which had been ordered for this task was received shortly before the end of the contract period. A preliminary run has been made with this pulser. It seems to verify and, in fact, to magnify the presence of a decreased attenuation when the current pulse is coincident with the time of traversal of the InSb by the acoustic signal. However, the interpretation, analysis, and further exploitation and confirmation of these results are now beyond the scope of this report.

VI. HOT ELECTRON EFFECTS

As discussed in Section IV, the attenuation or amplification at low lattice temperatures is expected to be altered significantly by increases in electron temperature due to applied electric fields[18,19]. Effects due to hot electrons are most evident from studies of electrical conductivity at high electric fields and low lattice temperatures[20-24].

Such increases in electron temperature are related to the rate of energy loss associated with the scattering mechanism. At low temperatures, ionized and neutral impurity scattering are the predominant processes for momentum transfer which in turn is responsible for the behavior of electrical conductivity. Although the momentum transfer per collision may be high, the fractional energy loss per collision will be quite small, however, due to the relatively large mass of the scattering center. Thus, energy supplied to electrons by

---

* Cober Electronics, Inc. Stamford Connecticut 06902

the external field is readily randomized by the scattering process and the result is an elevation of electron temperature. Under these conditions, the electron system is weakly coupled thermally to the lattice. At higher lattice temperatures, thermal coupling between electrons and lattice is enhanced by phonon interactions hence the electron and lattice temperatures never separate appreciably and consequently hot electron effects become insignificant.

A rise in electron temperature is manifested at low lattice temperature as an increase in the observed conductivity or mobility. That the mobility should increase with increasing fields is evident from the dependence of mobility on lattice temperature at low field strengths.

The mobility is calculated by averaging the relaxation time for momentum transfer over the (electron) distribution function. For impurity scattering, the relaxation time is essentially independent of lattice temperature in contrast to the situation at higher lattice temperatures where phonon scattering dominates and the relaxation time has an inverse dependence on lattice temperature[25]. Averaging the relaxation time for impurity scattering over the (non-degenerate) distribution function yields the well known increasing temperature dependence: $\mu \sim T^{-3/2}$, where T represents the temperature of the electron distribution.

Measurements of mobility at low fields represent a situation where electrons are in equilibrium with the lattice ($T = T_2$) and thus

the observed variation of mobility with lattice temperature is actually a measure of the dependence of mobility on electron temperature. In other words, if the lattice temperature were to remain fixed, the increase of mobility with electron temperature would be identical to the results obtained at vanishingly small fields by varying the lattice temperature.

It is evident that the mobility may be regarded as a thermometer for electron temperature whose calibration may be determined experimentally by measuring conductivity or mobility as a function of lattice temperature at very low field strengths. The electron temperature determined at higher field strengths may be used in theoretical predictions for the dependence of attenuation on electric field.

To verify the magnitude of hot electron effects, and to obtain suitable data for predicting attenuation and amplification, a series of conductivity measurements was carried out on a high purity sample of InSb* removed from the ingot intended for phonon transmission measurements (Ingot E). The conductivity was measured at fields up to 0.2 v/cm using an AC bridge and by pulse techniques up to 250 v/cm at lattice temperatures from 4.2 to 20°K. The observed zero-field mobility vs. temperature is given in Fig. 11, and the effects of electron heating are presented in Fig. 10. From these measurement, the dependence of electron temperature on applied field were extracted (Fig. 15). An interesting by-product of these results is the determination of the time constant for energy loss.

---

* $n = 1 \times 10^{14}$ cm^{-3}

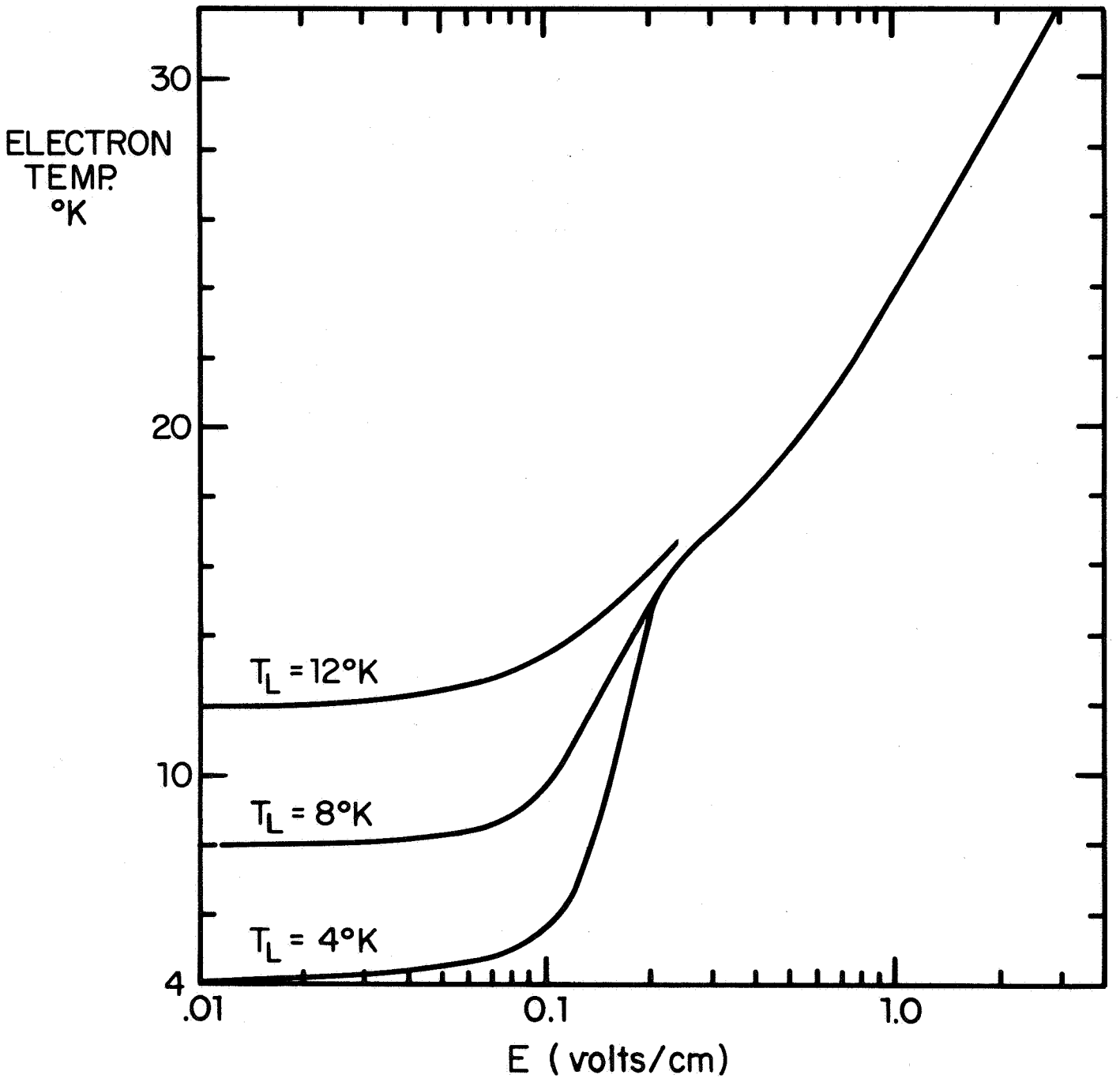

Figure 15 - Electron temperature dependence on applied electron field deduced from mobility vs. lattice temperature data of Figure 11 and mobility vs. electric field data of Figure 10.

The power density supplied by the field to the crystal is given by the relation:

$$P = \sigma E^2$$

where σ is the electrical conductivity and E the electric field. If the electron system is sufficiently thermalized to have a characteristic temperature, its heat content may be represented in the non-degenerate case by the usual term $U = \frac{3}{2} NKT$ where N represents the carrier density. The relaxation time for energy loss may be defined by:

$$\tau_e = \frac{dU}{dP} = \frac{3}{2} NK \frac{dT}{dP}$$

or

$$\tau_e = \frac{3}{2} NK \frac{dT}{d(\sigma E^2)}$$

Using the measured conductivities and derived electron temperature, the data shown in Figs. 10 and 15 were processed to calculate τ_e for three lattice temperatures $4^\circ K$, $8^\circ K$ and $12^\circ K$. The results are presented in Fig. 16. The relaxation time is observed to be relatively insensitive to lattice temperature variation, as expected.

A striking feature of the relaxation time is its strong electron temperature dependence. At higher temperatures, this is due mainly to the onset of polar optical scattering as may be seen by comparison to a prediction based on the work of Stratton[26] using a characteristic temperature of $260^\circ K$. The deviation from the data at higher temperatures is believed due mainly to the failure of an approximation used in the calculation. At $4^\circ K$, the data is in good agreement with the

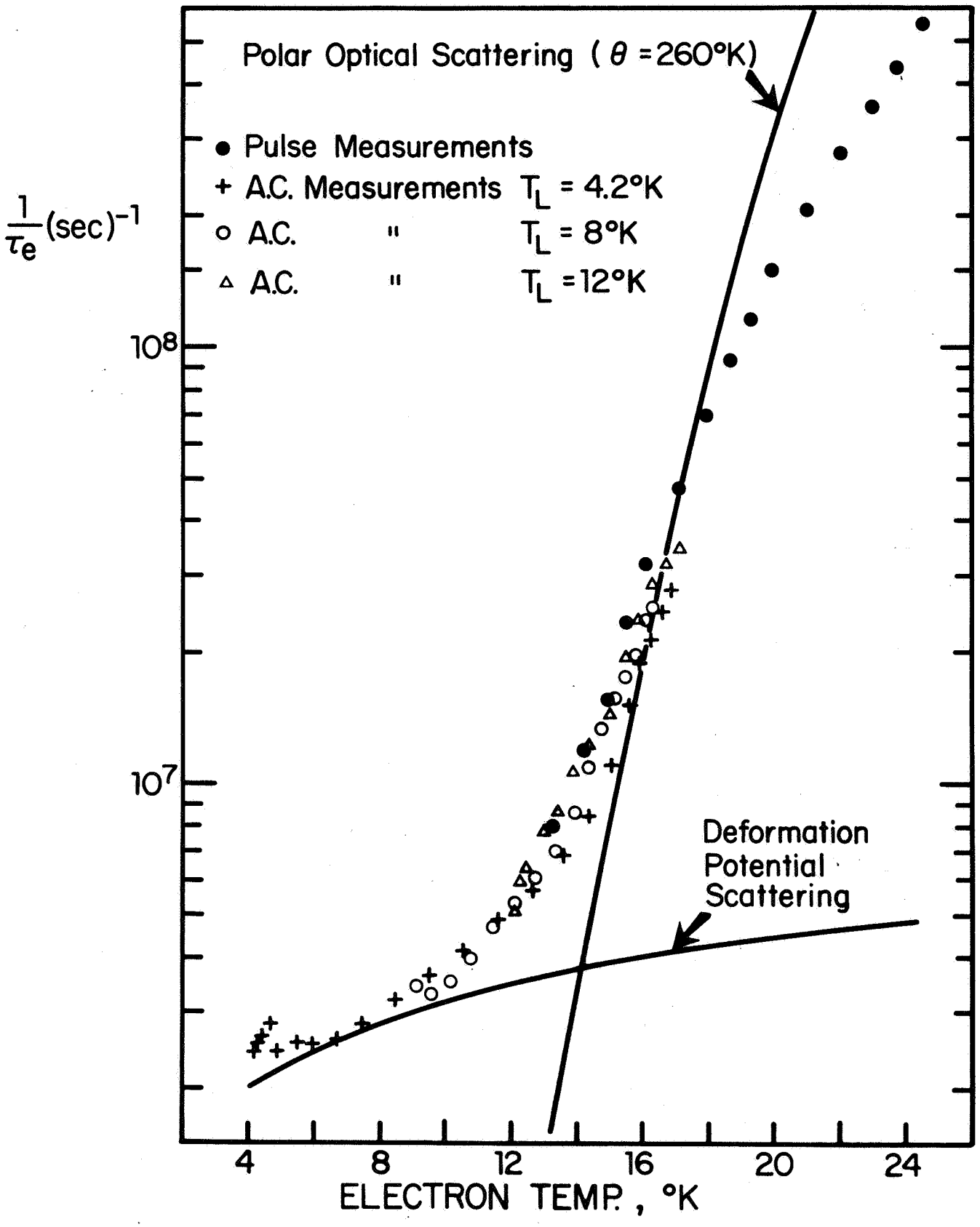

Figure 16 - Energy relaxation time for electrons to the lattice calculated from mobility measurements at three lattice temperatures 4.2°, 8° and 12°K.

results of Peskett and Rollin[21] $\tau_e = 3 \times 10^{-7}$ sec. At higher temperatures, the agreement with predictions of polar optical scattering is a considerable improvement over results found by Sandercock[20]. Values for τ_e at temperatures of 4-12°K appear to be in reasonable agreement with predictions based on deformation potential scattering[27] yielding a deformation potential of ~ 20 ev. The deformation potential so derived appears to be less than the results of Haga and Kimura[28] and somewhat larger than the values of 7 ev found by Sladek[24] and 4.5 ev found by Nill[17].

VII. SUMMARY AND CONCLUSIONS

A method of preparing semiconductor samples for acoustic propagation studies involving the electron-phonon interaction was evolved. This method consisted primarily of crystallographic alignment of the ingot using x-ray techniques followed by lapping and polishing to produce optically flat, parallel and smooth surfaces normal to the chosen crystallographic axis. The ingot thus prepared was then cut into rods for use in the microwave ultrasonic system. Piezoelectric transducers were attached to these rods; either a quartz rod was epoxy bonded to the rod with a special joining technique or a cadmium sulfide film was vapor deposited on the surface.

The cadmium sulfide vapor deposition method of deKlerk[14] was adapted for use with these semiconductor rods. This method involved the use of a quartz crystal microbalance developed to measure the film thickness and growth rate. The growth rate was kept below 5 Å/min as determined by the microbalance. It was found that control of the cadmium vapor pressure was the determing factor in controlling the growth

rate since the sulfur tended to diffuse readily but did not deposit on the warm surfaces without cadmium.

The cleaning procedure was found to be very critical for film growth. In the chemical cleaning before inserting the substrates into the vacuum system final wash in specially clean Freon-cleaning agent was necessary to eliminate unwanted deposits. The ion-bombardment cleaning had to be done by indirect bombardment to prevent cathodic sputtering of the substrate surface and the microbalance crystal and also to avoid contaminant buildup on the surface. The introduction of a regulated leak of dry air into the system during ion bombardment proved essential for production of consistently clean surfaces.

The RIAS electron microscope was used to evaluate the orientation of the films by reflection electron diffraction. It was found that the smoothness of the substrate surface was critical for growth of an oriented CdS film. InSb surfaces polished for flatness and parallelism and deemed sufficiently smooth for acoustic reflection were found to be not satisfactory for oriented film growth. Further polishing to a high mirror finish was necessary.

Up to the writing of this report the cadmium sulfide films produced on z-cut quartz rods (which are non-piezoelectric along the z-axis) were about 10 db less efficient in round trip transducer efficiency than were x-cut quartz transducer rods. Acoustic echoes were not observed from InSb rods upon which CdS films were deposited even after the improved surface polishing. One of these InSb rods did yield acoustic echoes 17 db above the noise when an x-cut quartz transducer was bonded to it. The 10 db loss of efficiency for the CdS films as

compared to x-cut quartz plus a 55% worsening of the cavity Q during insertion of InSb could account for this lack of echoes.

The principal theories of electron-phonon interaction applicable to these experiments were examined and compared. Some small discrepancies were found between some of the expressions from different theories but generally they agreed very well with each other. It was shown that the difference between the theory for degenerate statistics and for non-degenerate statistics lay in the equivalence of the mean electron energy terms; $\frac{1}{2} mv_F^2$ for the degenerate case and $\frac{3}{2} KT$ for the non-degenerate cases.

The effects of electron heating on the mobility of electrons in InSb were measured and used to calculate the effect of this heating on the acoustic grain predicted by these theories.

The same data were used with a relaxation time model for energy loss from the electrons to the lattice to obtain values of relaxation time as a function of electron temperature. These values were seen to indicate a predominance of energy loss by polar optical scattering at electron temperatures above $\sim 14^{\circ}K$ while deformation potential scattering seemed to dominate at lower temperatures. The striking feature of these results was that the values for relaxation time, τ_e, were independent of lattice temperature even when the electron temperature exceeded the lattice temperature considerably (e.g. $T_L = 4^{\circ}K$ and $T_e = 17^{\circ}K$ gives the same result as $T_L = 12^{\circ}K$ and $T_e = 17^{\circ}K$).

Analysis of previous data on temperature variation of acoustic attenuation in InSb yielded a value of 12 db/cm for the absolute value

of attenuation due to electron-phonon interaction at $4.2^{o}K$ and a value of $K^2 = 3.3 \times 10^{-4}$ for the acoustoelectric coupling coefficient for 9.3 GHz acoustic waves in the (111) direction. This lattice measurement is in good agreement with a magnetoacoustic determination of K^2 by Nill[17].

Repeated attempts at propogating acoustic waves through InSb rods demonstrated the need for the improved transducer bonding method adopted during the later portions of this work. With this method, usable acoustic reflections were obtained for the first time in an InSb rod which was long enough to attach electrical contacts. Electrical pulses were applied to these contacts during the transit of the acoustic wave through the InSb crystal. A marked increase in pulse amplitude was noted when such a pulse was applied in some preliminary tests with this crystal. However, the analysis, interpretation and further investigation of these results are now beyond the scope of this report.

REFERENCES

1. H. N. Spector, "Amplification of Acoustic Waves through Interaction with Conduction Electrons", Phys. Rev. 127, 1084 (1962).

2. N. Mikoshiba, "Interaction of Conduction Electrons with Acoustic Waves in Simple Semiconductors", J. Phys. Soc. Japan 15, 982 (1960).

3. S. G. Eckstein, "Resonant Amplification of Sound by Conduction Electrons", Phys. Rev. 131, 1087 (1963).

4. Y. A. Chikvashuili, "Theory of the Absorption of Sound in Semiconductors", Soviet Phys. Solid State 5, 264 (1963).

5. E. P. Pokatilov, "Resonance Absorption of High Frequency Sound Energy by Semiconductor Current Carriers in a Magnetic Field", Soviet Phys. JETP 11, 835 (1960).

6. D. L. White, "Amplification of Ultrasonic Waves in Piezoelectric Semiconductors", J. Appl. Phys. 33, 2547 (1962).

7. A. R. Hutson, J. H. McFee and D. L. White, "Ultrasonic Amplification in CdS", Phys. Rev. Letters 7, 237 (1961).

8. F. S. Hickernell, "The Electroacoustic Gain Interaction in III-V Compounds: Gallium Arsenide", IEEE Trans. Sonics & Ultrasonics SU-13, 73 (1966).

9. M.Pomerantz, "Amplification of Microwave Phonons in Germanium", Phys. Rev. Letters 13, 308 (1964).

10. J. P. Martin, "Study of Electron-Phonon Interactions in III-V Semiconductors", RIAS Technical Report, Contract NAS-8-20012, June 1966, Control Number DCN 1-5-28-01001-01(IF).

11. M. Pomerantz, "Temperature Dependence of Microwave Phonon Attenuation", Phys. Rev. 139, A501 (1965).

12. R. Nava, R. Azrt, I. Ciccarello and K. Dransfeld, "Hypersonic Absorption in Quartz at Temperatures Below 30°K", Phys. Rev. 134, A581 (1964).

13. Humphrey J. Maris, "On the Mean Free Path of Low Energy Phonons in Single Crystal Quartz", Phil. Mag. 9, 901 (1964).

14. J. deKlerk and E. F. Kelly, "Vapor-Deposited Thin-Film Piezoelectric Transducers", Rev. Sci. Inst. 36, 506 (1965), also J. deKlerk, "Fabrication of Vapor-Deposited Thin Film Piezoelectric Transducers for the Study of Phonon Behavior in Dielectric Materials at Microwave Frequencies in Physical Acoustics", edited by W. P. Mason Vol. IV-A, Chap. 5 (1966).

15. L. Holland, "The Cleaning of Glass in a Glow Discharge", Brit. J. Appl. Phys. 9, 410 (1958); "The Effects of Glow Discharge on Glass and Organic Materials" Advances in Vacuum Science & Technology, edited E. Thomas Vol. II, 753 (1960).

16. A. B. Pippard, "Ultrasonic Attenuation in Metals", Phil. Mag. 46, 1104 (1955).

17. K. W. Nill and A. L. McWhorter, "Magneto-Acoustic Effects in n-InSb at 9 GHz", J. Phys. Soc. Japan 21 (Suppl.) 755 (1966).

18. H. E. Pauwels, "Possibilities of Amplification of Sound Waves at Microwave Frequencies", Proc. IEEE 52, 300 (1964).

19. E. M. Conwell, "Amplification of Acoustic Waves at Microwave Frequencies", Proc. IEEE 52, 964 (1964).

20. J. R. Sandercock, "Energy Exchange between Hot Carriers and the Lattice in Indium Antimonide", Proc. Phys. Soc. 86, 1221 (1965).

21. G. D. Peskett and B. V. Rollin, "Energy Exchange between Hot Carriers and the Lattice in Indium Antimonide", Proc. Phys. Soc. 82, 467 (1963).

22. E. H. Putley, "Electrical Conduction in n-Type InSb between 2°K and 300°K", Proc. Phys. Soc. (London) 73, 280 (1959).

23. M. A. Kinch, "Scattering Mechanisms in Indium Antimonide at Low Temperatures", Brit. J. Appl. Physics 17,1257 (1966).

24. R. J. Sladek, "Quadratic Deviations from Ohm's Law in n-Type InSb", Phys. Rev. 120, 1589 (1960).

25. F. J. Blatt, "Theory of Mobility of Electrons in Solids", Solid State Physics, Vol. 4, p. 240, Academic Press (1957).

26. R. Stratton, "The Influence of Interelectronic Collisions on Conduction and Breakdown in Polar Crystals".

27. Sh. M. Kogan, "On the Theory of Hot Electrons in Semiconductors" Soviet Physics, Solid State 4, 1813 (1963).

28. E. Haga and H. Kimura, "Free-Carrier Infrared Absorption and Determination of Deformation-Potential Constant in n-Type InSb", J. Phys. Soc., Japan 18, 777 (1963).